

N72. 32801

NASA TECHNICAL NOTE



NASA TN D-6979

NASA TN D-6979

CASE FILE
COPY

APOLLO COMMAND MODULE LAND-IMPACT TESTS

by J. E. McCullough and J. F. Lands, Jr.
Manned Spacecraft Center
Houston, Texas 77058



1. Report No. NASA TN D-6979	2. Government Accession No.	3. Recipient's Catalog No.	
4. Title and Subtitle APOLLO COMMAND MODULE LAND-IMPACT TESTS		5. Report Date October 1972	6. Performing Organization Code
		8. Performing Organization Report No. MSC S-301	
7. Author(s) J. E. McCullough and J. F. Lands, Jr., MSC		10. Work Unit No. 914-50-20-17-72	11. Contract or Grant No.
9. Performing Organization Name and Address Manned Spacecraft Center Houston, Texas 77058		13. Type of Report and Period Covered Technical Note	
		14. Sponsoring Agency Code	
12. Sponsoring Agency Name and Address National Aeronautics and Space Administration Washington, D. C. 20546		15. Supplementary Notes The MSC Director waived the use of the International System of Units (SI) for this Technical Note because, in his judgment, the use of SI Units would impair the usefulness of the report or result in excessive cost.	
16. Abstract Full-scale-model and actual spacecraft were impact tested to define the emergency land-landing capability of the Apollo command module. Structural accelerations and strains were recorded on analog instrumentation, and a summary of these data is included. The landing kinematics were obtained from high-speed photography. Photographs of the structural damage caused during the tests are included. Even though extensive structural damage can be expected, the crew will receive nothing more than minor injuries during the majority of the probable landing conditions.			
17. Key Words (Suggested by Author(s)) · Land Impact · Apollo Command Module · Emergency Landing · Crew Accelerations		18. Distribution Statement	
19. Security Classif. (of this report) None	20. Security Classif. (of this page) None	21. No. of Pages 61	22. Price \$3.00

CONTENTS

Section	Page
SUMMARY	1
INTRODUCTION	1
PROGRAM OBJECTIVES	2
LANDING SURFACE	3
John F. Kennedy Space Center Terrain Survey	3
Manned Spacecraft Center Impact Surface	3
TEST FACILITY	5
Launching Equipment	5
Facility Operation	7
TEST VEHICLES	7
Boilerplate Structures	7
Spacecraft Structures	8
Secondary Spacecraft Equipment	11
Crew-Systems Equipment	12
TEST INSTRUMENTATION	15
Photography	15
Instrumentation	16
TEST RESULTS	17
Comparison of the Kennedy Space Center and Manned Spacecraft Center Impact Surfaces	17
Comparison of Kennedy Space Center Terrain Types	18
Manned Spacecraft Center Test Program	19
Tests at 0° Roll	20
Tests at 180° Roll	25

Section	Page
Askew Landing Tests	36
Damage to Secondary Equipment	37
Crew-Systems-Equipment Performance	39
Structural Capability and Stability	41
Probability of Emergency Landing	41
CONCLUDING REMARKS	42
APPENDIX A — INSTRUMENTATION	43
APPENDIX B — IMPACT DATA	52

TABLES

Table		Page
I	LABORATORY COMPARISONS OF SELECTED SAND SAMPLES	4
II	CREW-COUCH DATA AND STRUT STROKES	14
III	STROKING LOADS OF CREW-COUCH STRUTS	15
IV	IMPACT-TEST CONDITIONS AND ACCELERATIONS	18
B-I	APOLLO COMMAND MODULE IMPACT TESTS	52

FIGURES

Figure		
1	Launch complexes 39A and 39B at the KSC	2
2	Comparison of the KSC and MSC impact-surface sands	4
3	Impact soil bearing pressures	5
4	Monorail and accelerator rails	6
5	Accelerating components of launching catapult	
	(a) Monorail trolley supporting a test vehicle	6
	(b) Acceleration pusher assembly cradling a test vehicle	6
6	Apollo CM structural configuration	8
7	Views of BP-1201	
	(a) Exterior view	8
	(b) Interior view	8
8	Apollo CM dimensions	9
9	Exterior view of Block I CM	9
10	The CM docking tunnels, -Z side	
	(a) Block I	10
	(b) Block II	10

Figure	Page	
11	The RCS tanks and clearances	
	(a) Plan view of tanks looking aft	11
	(b) Clearance between tanks and ballast	11
12	View of oxygen surge tank	12
13	Apollo CM impact system	12
14	Crew-couch systems	
	(a) Unitized crew couch	13
	(b) Foldable couch	13
15	Comparison of honeycomb and cyclic couch struts	
	(a) Honeycomb strut	14
	(b) Cyclic strut	14
16	Photoinstrumentation system in test vehicle	15
17	Boilerplate c. g. accelerations on the KSC and MSC impact surfaces	
	(a) BP-25 at the MSC	17
	(b) BP-25 at the KSC	17
	(c) BP-1201 at the MSC	18
18	Center-of-gravity accelerations from 38-fps and 32-fps vertical velocities	
	(a) Vertical velocity of 38 fps in test 81	19
	(b) Vertical velocity of 32 fps in test 80	19
19	Landing dynamics during a 0° roll test	20
20	Boilerplate accelerations as a function of horizontal velocity	22
21	Boilerplate accelerations as a function of pitch attitude	22
22	Comparison of spacecraft and boilerplate accelerations	22
23	Accelerations from test 16 with BP-28A	23
24	Accelerations from test 31 with CM-009	23
25	Impact damage to CM-009 in test 31	24

Figure	Page	
26	Factors in the dynamics of a CM landing	
	(a) Landing at 0° roll	25
	(b) Landing at 180° roll	25
27	Theoretical trajectory of CM c. g. during a 180° roll impact	26
28	Landing dynamics of CM-008 during test 28	27
29	Impact damage to CM-008	27
30	Landing dynamics of CM-009 during test 63	29
31	Damage to CM-009 during a 180° roll landing	30
32	Landing dynamics of CM-011 during test 64	32
33	Impact damage to CM-011	32
34	Accelerations at c. g. recorded during test 28 with CM-008	34
35	Boilerplate c. g. accelerations under conditions of test 28	34
36	Accelerations at c. g. during test 63 with CM-009	34
37	Boilerplate accelerations at c. g. under conditions of test 63	35
38	Accelerations at c. g. during test 64 with CM-011	35
39	Boilerplate accelerations under conditions of test 64	36
40	Accelerations recorded during test 68 with CM-002B	36
41	Boilerplate accelerations under conditions of test 68	36
42	Landing dynamics of CM-002B during test 68	37
43	Damage to CM-002B in test 68	37
44	Typical impact damage to RCS tanks	38
45	Accelerations in the X axis during test 31 with CM-009	40
46	Accelerations in the X axis during test 64 with CM-011	40
47	Land-landing capability as a function of roll angle of a CM	41
A-1	Locations of accelerometers and stroke indicators for test 16 with BP-28A	43

Figure	Page
A-2 Aft-sidewall strain-gage locations for test 16 with BP-28A	43
A-3 Details of aft-sidewall strain-gage locations for test 16 with BP-28A	44
A-4 Aft-sidewall strain gages at core 2 for test 16 with BP-28A	44
A-5 Aft-sidewall strain gages at core 3 for test 16 with BP-28A	44
A-6 Aft-bulkhead equipment and instrumentation for test 16 with BP-28A	44
A-7 Range-camera coverage for test 16 with BP-28A	45
A-8 Locations of structural accelerometers for test 28 with CM-008	45
A-9 Instrumentation of foldable crew couch and support system for test 28 with CM-008 and test 31 with CM-009	45
A-10 Locations of analog-recorded strain gages for test 28 with CM-008	
(a) Inside view toward +Z	46
(b) Inside view toward -Z	46
A-11 Locations and views of range cameras for test 28 with CM-008	46
A-12 Locations of structural accelerometers for test 31 with CM-009	47
A-13 Locations of sidewall- and aft-bulkhead strain gages for test 31 with CM-009	47
A-14 Locations of side-frame strain gages for test 31 with CM-009	48
A-15 Locations of range cameras for test 31 with CM-009	48
A-16 Structural accelerometers for test 63 with CM-009 and test 64 with CM-011	48
A-17 Crew-couch accelerometers for test 63 with CM-009 and test 64 with CM-011	48
A-18 Crew-couch strut instrumentation for test 63 with CM-009	49
A-19 Locations of range cameras for test 63 with CM-009	49
A-20 Crew-couch strut instrumentation for test 64 with CM-011 and test 68 with CM-002B	50

Figure		Page
A-21	Locations of range cameras for test 64 with CM-011	50
A-22	Structural accelerometers for test 68 with CM-002B	51
A-23	Crew-couch instrumentation for test 68 with CM-002B	51
A-24	Locations of accelerometers in BP-1201	51

APOLLO COMMAND MODULE LAND-IMPACT TESTS

By J. E. McCullough and J. F. Lands, Jr.
Manned Spacecraft Center

SUMMARY

A low-altitude or pad abort can result in a land landing of the Apollo command module. An extensive investigation was performed to identify potential crew hazards associated with land landing.

A 10-mile radius of the launch area was inspected, and the percentage area of each terrain type was determined. The relevant soil properties of each terrain type were measured. Full-scale boilerplate vehicles then were impact tested at the launch area at the NASA John F. Kennedy Space Center and on a simulated test bed at the NASA Manned Spacecraft Center. The impact tests were designed to establish the combinations of spacecraft attitude and velocity that produced the most severe vehicle dynamics and to verify the acceptability of the simulation at the Manned Spacecraft Center of the launch-area soil.

The boilerplate tests were followed by impact tests of spacecraft structures. The tested structures contained all the significant secondary equipment, crew-station equipment, and anthropomorphic dummies. All spacecraft structures were instrumented extensively with strain gages and accelerometers. Six spacecraft tests were conducted: two at 0° roll, three at 180° roll, and one at an askew roll of 325° . In all tests, the vertical velocity at impact was 32 fps, which simulated a nominal three-parachute landing. The horizontal velocity was varied from 20 to 54 fps, the latter being the wind velocity that constrains the launch of the booster. Landings with the spacecraft at a roll orientation of 180° were the most unstable and tumbled the vehicle, producing multiple impacts. Higher horizontal velocities produced more violent impacts.

The damage to spacecraft structures was extensive and included compartment sidewall cracks and debonding of secondary equipment. However, at horizontal velocities less than 40 fps, the crew has an excellent chance for survival. Potential hazards to the crew were the possible rupture of the fuel and oxidizer tanks and the high accelerations recorded at the crew-couch system. In general, however, the Apollo command module and associated components withstood severe landings better than had been expected.

INTRODUCTION

The Apollo earth-landing system was developed for water landings. However, the locations of launch pads 39A and 39B at the NASA John F. Kennedy Space Center (KSC)

(fig. 1) and the high probability of onshore, or easterly, winds result in an 83-percent chance of a land landing should an abort occur from a pad or during the first 40 seconds of flight.

To define the land-landing capability of the Apollo command module (CM), a program was initiated during 1967 at the NASA Manned Spacecraft Center (MSC). The program consisted of terrain studies in the vicinity of the KSC launch pads, the establishment of an impact-testing facility at the MSC, impact tests of full-scale boilerplate (BP) command modules, impact tests of actual spacecraft, and analysis of the data collected from test instrumentation. Fifty-one impact tests were made with boilerplate vehicles to qualify the facility and to determine conditions for the spacecraft tests. Six impact tests were made with representative Apollo command modules.

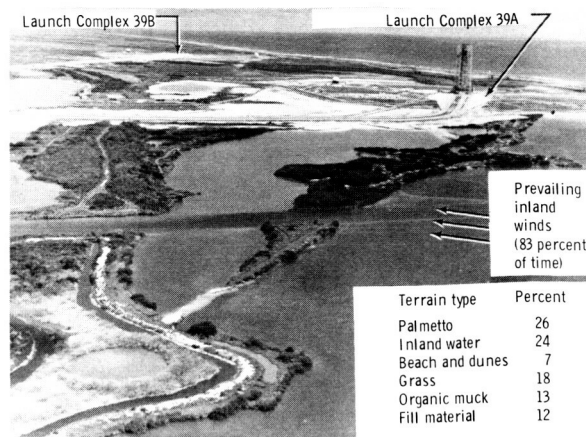


Figure 1. - Launch complexes 39A and 39B at the KSC.

The investigative program, specific objectives, test facilities, test vehicles and equipment, and test results are described in this report. Summaries of data obtained from individual tests are included to clarify or augment stated test results.

PROGRAM OBJECTIVES

The program consisted of a series of related objectives and tests. A terrain survey of the KSC launch area identified the types of terrain upon which a pad abort might occur. Then, a series of boilerplate command module impact tests established the severity of landings on the various types of terrain. An impact surface that was representative of the most severe KSC landing surface was constructed at the MSC and was verified by soil and boilerplate impact tests. Then, the combinations of spacecraft attitude and velocity that produced the most severe dynamics on impact were established. Finally, actual spacecraft were tested under the most severe conditions to determine potential crew hazards.

The specific objectives of the impact-test program were as follows.

1. To define the capability of the CM structures to withstand a land landing
2. To measure the accelerations that would be experienced on the CM structure and by the crewmen
3. To identify hazards presented by flight hardware during a land landing, including damage to reaction control system (RCS) tanks and plumbing, damage to the oxygen surge tank, and dislodged hardware within the crew compartment
4. To determine the vehicle landing dynamics and any associated difficulties in crew recovery

LANDING SURFACE

John F. Kennedy Space Center Terrain Survey

To evaluate possible landing sites, a field study of the KSC launch area was made between October 2 and November 28, 1967. During the survey, the area was mapped, the relative proportions of soil and vegetation types were determined, and the critical mechanical properties of the soil types were measured.

In the site survey, six basic types of terrain were identified. The terrain types and the relative proportions within the launch area are as follows.

<u>Terrain type</u>	<u>Area, percent</u>
Palmetto	26
Water	24
Grass	18
Organic muck	13
Fill material	12
Beach and dunes	7

The palmetto terrain was relatively dry sand overgrown with thick underbrush and palmetto vegetation. The water sites were shallow-water marshes and ponds. The grass sites were sandy soils covered by salt grass 2 to 3 feet in height. The organic muck occurred in tidewater marshes and was a silty, quicksand type of soil with a high moisture content and a low bearing strength. The fill material was a fine-grained sand pumped from canals to raise the surface level. When dry, this fill material had a high bearing strength. The areas in the immediate vicinity of the launch pads were composed of fill material. The last category, beach and dunes, was composed of loose, water-washed or wind-drifted sand. Because of the high bearing strength, the fill material was considered to be the most formidable impact surface on which a spacecraft could land.

Manned Spacecraft Center Impact Surface

A sand material from the area of League City, Texas, was found to have properties similar to the fill material at the KSC. Comparisons of the properties of the League City and the KSC sands are presented in table I and in figure 2.

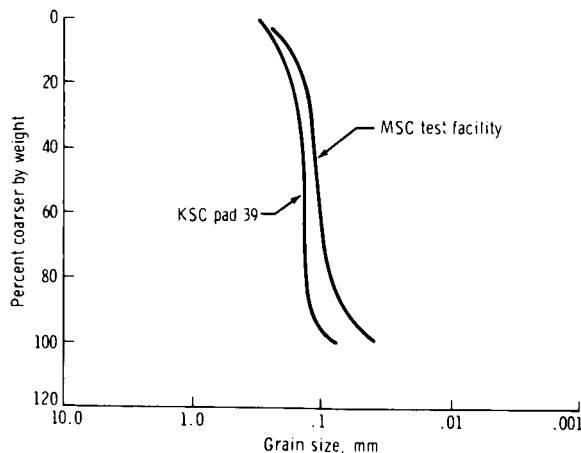
An impact surface was constructed at the MSC by filling a pit with the League City sand. The pit was 13 feet deep, 40 feet wide, and 100 feet long. To obtain the proper density, the sand was placed in the pit in 6-inch layers and then rolled before the application of another 6-inch layer. All subsequent surface-elevation changes during the test program were made by the same technique.

TABLE I. - LABORATORY COMPARISONS OF SELECTED SAND SAMPLES

Sample	Moisture, percent by weight	Angle of internal friction, deg	Cohesion, psi
League City, Texas	Room dry ^a	33.8	0.25
	5.5	32.2	.50
	10.0	33.1	.40
	20.0	32.7	.60
	30.5	30.7	.40
	^b 34.0	33.8	.00
KSC, west of pads 39A and 39B	Room dry ^a	37.8	0.20
	2.1	32.8	.30
	^b 37.8	37.6	.10
KSC, south of vertical assembly building	Room dry ^a	38.0	0.57
	^b 33.1	38.0	.27
KSC, Wilson Road	0.0	34.8	0.45
	6.2	33.5	.25
	^b 32.0	36.1	.00
KSC, beach area	0.0	33.1	0.26

^aRoom dry to less than 0.5 percent moisture content.

^bSaturated.



To prevent radical moisture-content changes between tests, the impact surface was covered with a plastic sheet. Immediately preceding each spacecraft or BP-28A test, the moisture content and the density of the soil were measured by means of standard laboratory techniques. The bearing strength also was measured before each of these tests by recording the load-penetration curve of an 8-inch-diameter disk forced into the sand. The average moisture and density values determined for the major tests are listed in the following table.

Figure 2. - Comparison of the KSC and MSC impact-surface sands.

Test	Vehicle	Moisture content, percent		Density, lb/ft ³
		by weight		
16	BP-28A	8.36		122
28	CM-008	11.96		127
31	CM-009	10.80		123
63	CM-009	9.96		125
64	CM-011	9.80		125
68	CM-002B	--		--

The soil bearing pressure, which was measured at various depths before each major test, is plotted in figure 3. The data define a band with a slope of 320 psi per inch of penetration depth and with a data-scatter bandwidth of approximately 60 psi. No soil measurements were made for test 68 because previous samples had demonstrated consistent values of moisture and density, and no significant precipitation had occurred since test 64.

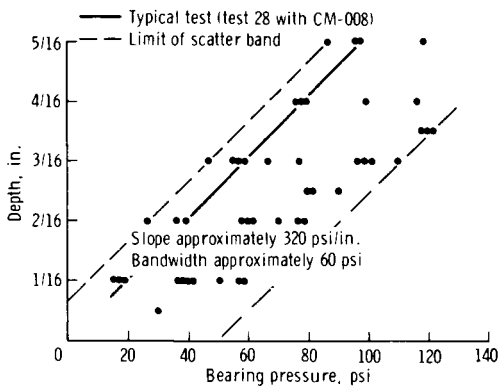


Figure 3. - Impact soil bearing pressures.

TEST FACILITY

Test facility 338 at the MSC was established in 1967 to impact test full-scale Apollo command modules on either water or land. The facility consisted of water- and land-impact areas arranged at opposite ends of a launching structure. The launching mechanism was a pneumatic catapult capable of propelling an Apollo-weight vehicle to a horizontal velocity of 65 fps at heights sufficient to obtain free-fall velocities as great as 40 fps. The facility also contained equipment for recording data from 200 channels of test instrumentation.

Launching Equipment

The launching equipment included an open-frame structure approximately 100 feet long to which a monorail and two accelerator rails were attached. The monorail supported a trolley from which the test vehicle was suspended. The attitude of the test vehicle was preset by adjusting the trolley and its rigging. The vehicle pusher assembly cradled the test vehicle at the specified attitude and, during acceleration, pushed the vehicle between the two accelerator rails. The pusher assembly was propelled by a cable system reeved 8 to 1 to a pneumatic cylinder the piston rod of which could stroke 11 feet. The major components of the facility are shown in figures 4 and 5. The moving components were equipped with a passive braking system consisting of a series of

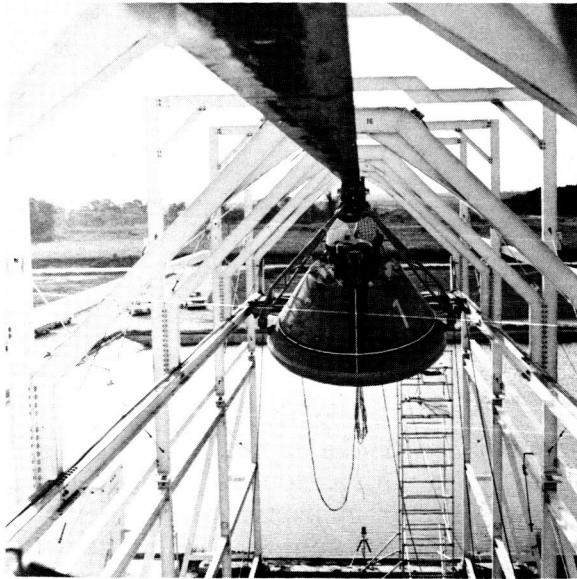
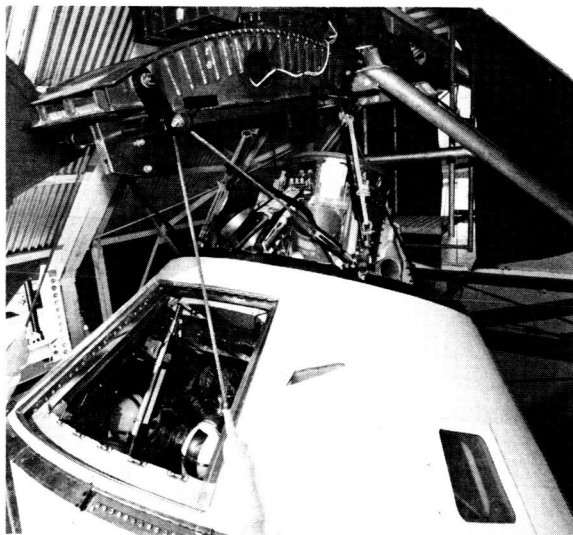


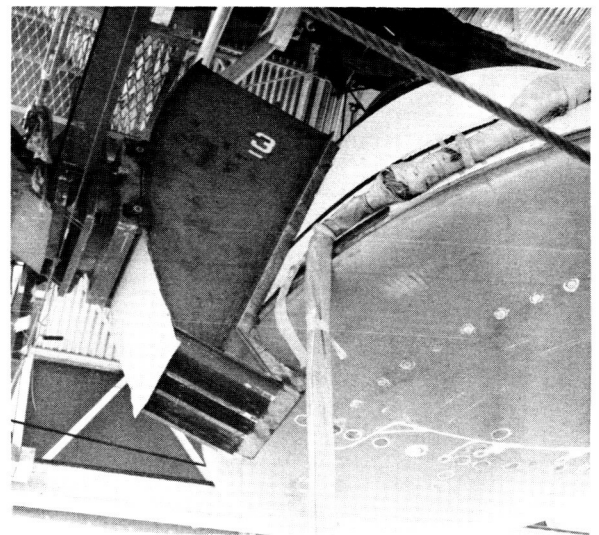
Figure 4. - Monorail and accelerator rails.

opposed, spring-loaded braking pads that were forced apart as the assembly contacted and overrode a tapered rail. A pyrotechnic device released the cables that suspended the test vehicle from the monorail trolley.

In operation, the trolley, the pusher assembly, and the test vehicle were accelerated to the desired velocity. The pusher was braked at the end of its run. Next, the test vehicle was released pyrotechnically from the trolley. Finally, the trolley was braked on its rail. The height of the fall, which determined the vertical velocity of the test vehicle, was adjusted by changing either the heights of the monorail and accelerator rails in the structure or by changing the height of the landing surface.



(a) Monorail trolley supporting a test vehicle.



(b) Acceleration pusher assembly cradling a test vehicle.

Figure 5. - Accelerating components of launching catapult.

Facility Operation

The test facility was adjusted to provide the specified conditions for each test. The free-fall height was adjusted to control the vertical velocity at impact. The trolley and acceleration pusher were adjusted to provide the pitch and roll attitudes. The air-storage-tank pressure that propelled the pneumatic piston was adjusted to achieve the required horizontal velocity.

Because data recorders, pneumatic-piston start switches, photographic lighting, cameras, and the pyrotechnic release had to be coordinated to perform the test, a programmed electronic sequence was used. The following is a typical sequence of events.

1. All recording systems energized	T - 5 min
2. Start button depressed; countdown starts	T - 10 sec
3. Vehicle acceleration begins; all cameras start	T - 0
4. Trolley trips first velocity-recording switch	T + 5.068 sec
5. Pyrotechnic release fires and internal flash lighting begins	T + 5.28 sec
6. Impact occurs	T + 6.28 sec
7. Secondary impact occurs	T + 7.40 sec
8. Impact dynamics end	T + 9.4 sec
9. Cameras run out of film	T + 10 sec
10. Internal flash lighting ends	T + 11.78 sec

TEST VEHICLES

Boilerplate Structures

Two drop-test sequences using boilerplate vehicles were performed to support and complement the test of spacecraft structures. The first sequence verified the similarity of the MSC and KSC impact surfaces and determined the relative severity of a landing on the various types of terrain at the KSC. The second sequence provided parametric data necessary to establish impact conditions for the tests of spacecraft structures.

Two boilerplate test vehicles (BP-1201 and BP-25) were used as full-scale models of an Apollo (Block II) CM. The boilerplates were constructed with steel I-beam structures and 3/16-inch steel-sheet exterior facings. Sidewalls were supported by I-beam stringers, and the simulated heat shields were supported by radial I-beams. No attempt was made to simulate the inner structure or the secondary equipment of a CM except for the effect on total weight and inertias. The desired mass and inertias were obtained

by the installation of lead ballast. The mass properties of the boilerplate vehicles are as follows. (Coordinates are shown in figure 6.)

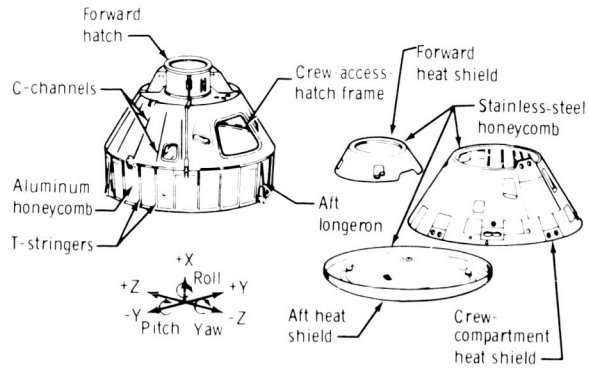
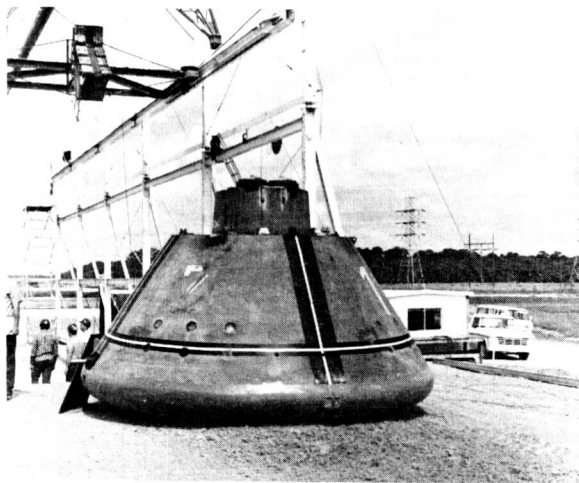


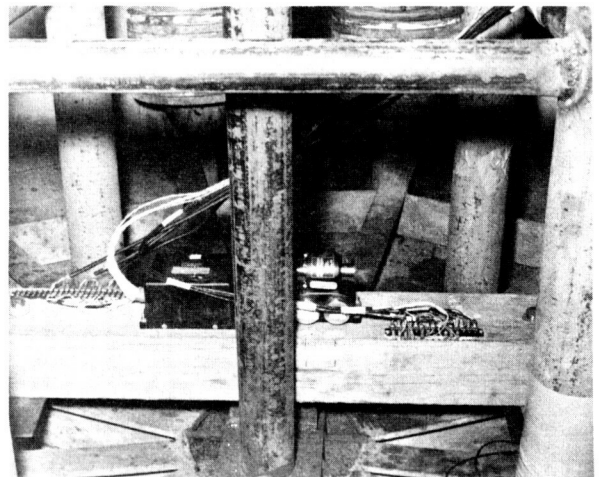
Figure 6. - Apollo CM structural configuration.

Weight, lb	12 720
Center of gravity, in.	
X_c	+38.5
Y_c	-0.02
Z_c	+4.6
Inertias, slug-ft ²	
I_{xx}	5650
I_{yy}	5097
I_{zz}	4420

In figures 7(a) and 7(b), exterior and interior views of BP-1201 are shown; BP-25 was similar to BP-1201.



(a) Exterior view.



(b) Interior view.

Figure 7. - Views of BP-1201.

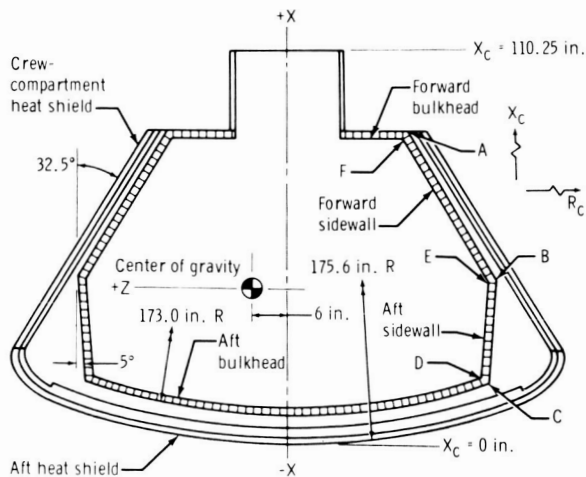
Spacecraft Structures

Basically, the Apollo CM is a structure within a structure. A trisegmented heat shield surrounds a pressurized crew compartment (fig. 6). The crew compartment is a 0.75- to 0.90-inch-thick sandwich structure composed of aluminum honeycomb with

bonded face sheets. The heat shield is fabricated of brazed stainless-steel honeycomb core and face sheets and varies in thickness from approximately 0.50 inch on the conical section to approximately 2 inches on the spherical section. Ablator material is bonded to the outer surface. The basic dimensions of the CM are shown in figure 8.

For economy, spacecraft structures that had been built for and tested in other ground- and flight-qualification programs were used in the land-impact program. The structures used included command modules CM-002B, CM-008, CM-009, CM-011, and boilerplate vehicle BP-28A. All command modules tested were of the Block I external configuration (fig. 9). The basic difference between the Block I spacecraft and the later Block II spacecraft was in secondary structure. Block I spacecraft were not designed for a lunar mission and, therefore, were not equipped with lunar module docking hardware. The docking hardware is in the forward region of the spacecraft. The two configurations are shown in figure 10. The aft heat shields and conical sidewalls of the configurations are similar.

The docking tunnel of a Block I spacecraft is a cylinder approximately 30 inches in diameter and 28.75 inches in height. The Block II tunnel is a truncated cone that is approximately 23 inches in height. Design differences also exist in the arrangement of the tunnel gussets, as shown in figure 10. The significant effect of the difference is that the docking tunnel of the Block II configuration has the higher load-carrying capability both in compression and in shear.



Location of points on structure, in.

Point	X_C	R_C
A	81.500	35.929
B	43.134	60.392
C	12.706	57.838
D	14.072	57.200
E	42.665	59.600
F	80.750	35.316

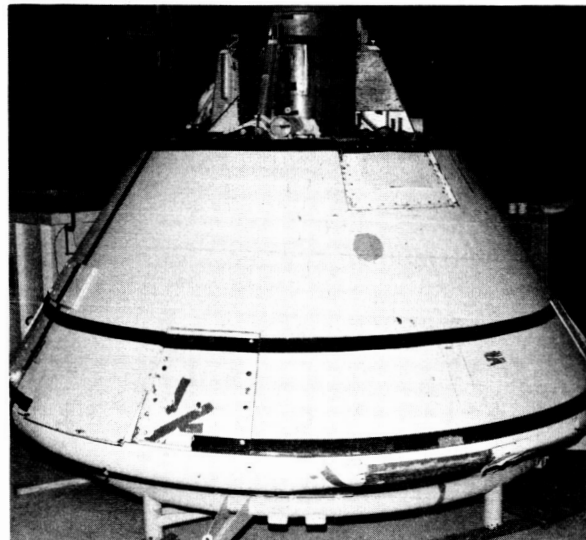
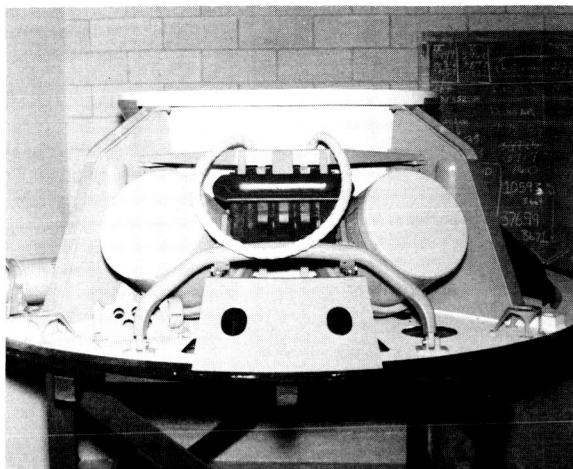
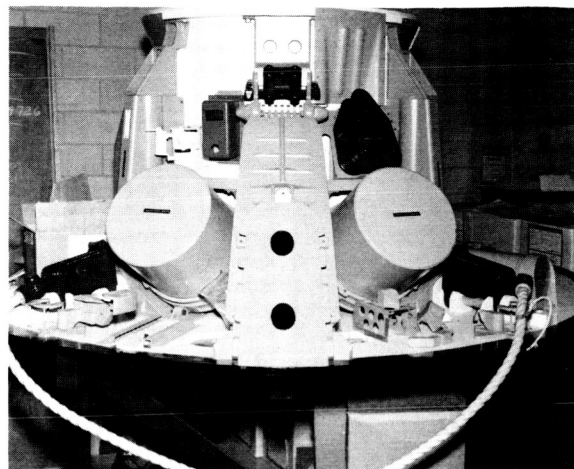


Figure 9. - Exterior view of a Block I CM.

Figure 8. - Apollo CM dimensions.



(a) Block I.



(b) Block II.

Figure 10. - The CM docking tunnels, -Z side.

An early design of the crew-compartment side hatch was incorporated in all the Block I vehicles tested. This design included an inner pressure hatch and a separate outer ablation hatch. The Block II design is a quick-opening, single-hinged hatch. The secondary equipment, including the main display console and all equipment bays, simulated the Block I configurations.

Test vehicle BP-28A was a hybrid structure. The upper or forward portion of the vehicle consisted of standard structural steel and aluminum members welded and bolted together. A spacecraft crew-compartment aft bulkhead and sidewall segment (120° section centered about the +Z axis) was attached to the boilerplate frame. A spacecraft aft heat shield was used. No secondary equipment other than a crew-couch system, the equipment installed in the lower bay, and the RCS tanks was represented.

Each spacecraft test vehicle used in the MSC land-impact tests was ballasted to a landing weight of 12 235 pounds, which represents a CM that weighs 13 500 pounds at launch. Test vehicles BP-28A, CM-008, and CM-009 (test 31) were ballasted to the following specifications.

Weight, lb	12 235 ± 100
Center of gravity, in.	
X_c	37.4 ± 1.0
Y_c	-0.5 ± 0.5
Z_c	5.9 ± 0.5
Inertias, slug-ft ²	
I_{xx}	5927
I_{yy}	5796
I_{zz}	5218

In March 1968, new predictions of the center-of-gravity (c. g.) location for the 13 500-pound launch weight were made, and the remaining tests (CM-009 in test 63, CM-011, and CM-002B) were conducted with the vehicles ballasted to the following specifications.

Weight, lb	12 235 ± 100
Center of gravity, in.	
X_c	38.5 ± 0.5
Y_c	0.0 ± 0.5
Z_c	4.7 ± 0.5
Inertias, slug-ft ²	
I_{xx}	5973
I_{yy}	5859
I_{zz}	5264

Secondary Spacecraft Equipment

Because one major concern for crew safety was the potential rupture of the RCS fuel and oxidizer tanks, these systems were simulated on all tests. However, only the associated plumbing in the immediate area of the tanks was included. Although the RCS tanks were not pressurized for any of the tests, for test 63, the tanks were filled with a Freon and isopropyl alcohol mixture to simulate the fuel and oxidizer masses.

The most probable cause of damage to the tanks is a puncture by the heat-shield ballast plates when the aft area deforms on impact. The ballast-plate installation is slightly different in each spacecraft depending on the extent to which the center of gravity must be adjusted. The locations of the RCS tanks in the spacecraft and the typical clearance between the tanks and the ballast are shown in figure 11.

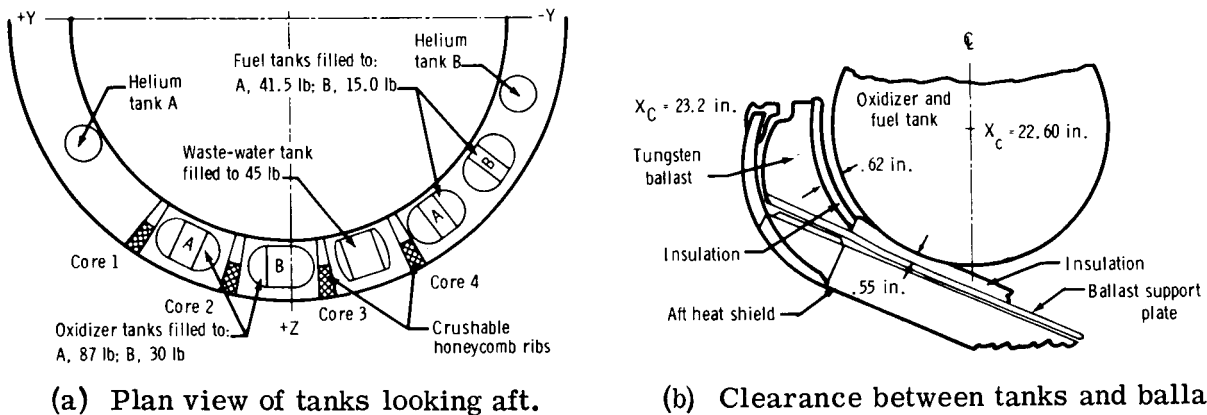


Figure 11. - The RCS tanks and clearances.

Another potential hazard to the crew during a landing is the oxygen surge tank, a thin-walled vessel that is normally pressurized to 850 psi. The oxygen surge tank was installed on all of the test spacecraft except BP-28A and was pressurized to 850 psi for test 63. The tank is approximately 15 inches in diameter and is located just behind the left-hand equipment bay in the -Z direction (fig. 12). The thin closeout panel would not provide much protection for the crew if the tank should fragment during impact.



Figure 12. - View of oxygen surge tank.

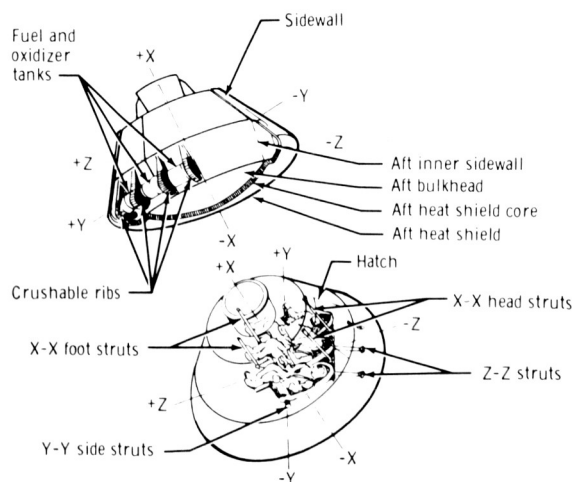


Figure 13. - Apollo CM impact system.

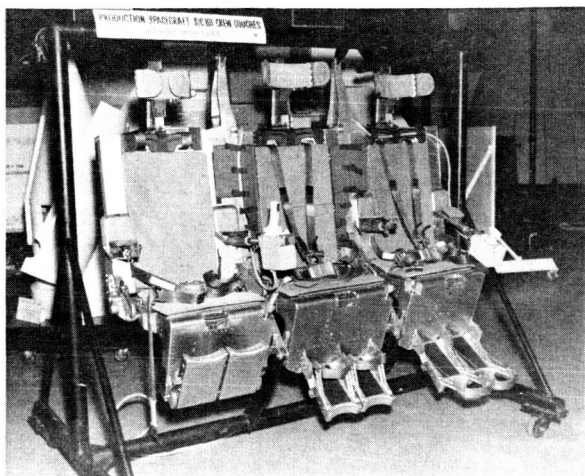
Crew-Systems Equipment

The Apollo CM impact system (fig. 13) consists of eight struts that support the crew couch and four aluminum honeycomb ribs in the lower +Z area of the CM structure. The CM structure and the landing surface absorb most of the impact energy. The eight impact-attenuation struts are identified in figure 13 by the relationship to the spacecraft axis in which the struts operate. The X-X head and foot struts are capable of strokes from the initial position of 16 inches in tension and 1 inch in compression. The Z-Z struts are capable of an 18.5-inch tension stroke and a 5-inch compression stroke from the initial position. The Y-Y struts have 4.5 inches of compression stroke and no tension capability. To accommodate crew-couch excursions experienced during the stroking of the X-X and Z-Z struts, the Y-Y struts have a ball-and-socket-mounted shoe that contacts a bearing plate mounted on each side of the crew compartment. The X-X and Z-Z couch struts are attached by spherical ball joints to the crew couch and to the structure of the CM.

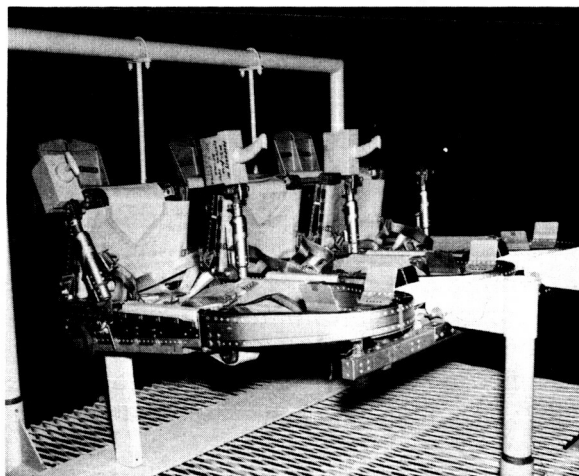
To improve equipment performance during an emergency land landing, the Apollo crew-systems equipment was modified several times during the course of the MSC impact-test program. The changes should be considered when comparisons are made of data from the various tests.

The first crew-systems equipment tested (in BP-28A) was a unitized crew couch supported by struts that absorbed energy by the crushing of honeycomb cores. The unitized crew couch (fig. 14(a)) consisted of three rigidly constructed couches fabricated of stiffeners and riveted face sheets. The

three couches were bolted together into a single unit that could not be disassembled easily in flight. Shortly after the BP-28A test, a change to a newly designed, foldable crew-couch system was initiated. The foldable couch system (fig. 14(b)) consisted of three independent couches, each composed of a lightweight, monocoque frame of sheet aluminum. A fiber body support was attached to the couch frame. During flight, each couch could be removed readily from its support frame to provide a larger working area for the crewmen.



(a) Unitized crew couch.

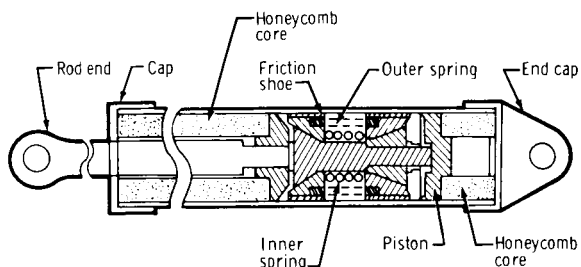


(b) Foldable couch.

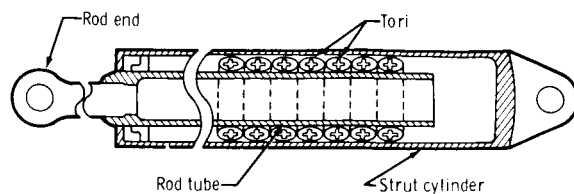
Figure 14. - Crew-couch systems.

The crew-couch struts used before and during the impact test of BP-28A absorbed energy by the crushing of a honeycomb core. These struts were designed to limit crew accelerations to approximately 20g and had mechanical lockout devices to prevent premature stroking during the deceleration phase of some atmospheric reentry conditions (fig. 15(a)). The lockout devices were deactivated before landing and, thus, were tested in the deactivated condition. It was discovered during the water-impact qualification program that even the most critical water landings failed to produce stroking of the couch struts. When it was realized that only emergency land impacts would cause the struts to stroke, the decision was made to increase the stroking loads of the Z-Z struts to a level producing emergency crew accelerations and thus to provide a higher energy-absorption capability.

To provide adjustable stroking loads, newly designed cyclic struts were incorporated into the system at the same time that the foldable couch was introduced. Both strut systems had the same attachment points. The cyclic struts could have their stroking loads tailored to fit individual crew weights and had energy absorption equally effective in both tension and compression, features not available with the honeycomb struts. A different metal-yielding technique was used to absorb energy in the cyclic strut. Small metal tori were twisted by the friction forces generated by their being in contact with an inner and an outer cylinder of the strut (fig. 15(b)). To reduce the stroking force, the number of tori were reduced.



(a) Honeycomb strut.



(b) Cyclic strut.

Figure 15. - Comparison of honeycomb and cyclic couch struts.

All of the spacecraft were tested with the foldable couch and the cyclic struts. The struts were designed to limit crew accelerations to 35g to 40g in the X axis and 18g to 20g in the Z axis. Accelerations exceeding those specified as emergency crew levels were recorded by the anthropomorphic dummies that were installed in the couch to simulate the mass of the crewmen. Then, the stroking loads of the struts were reduced in an attempt to decrease the X- and Z-accelerations to approximately 20g and 8g, respectively. Lockout devices again were incorporated in the design. However, they were not used in any of the tests discussed in this report. Crew-couch-system data, including couch-strut strokes and stroking loads, are presented in tables II and III.

TABLE II. - CREW-COUCH DATA AND STRUT STROKES

Item	Test 16, BP-28A	Test 28, CM-008	Test 31, CM-009	Test 63, CM-009	Test 64, CM-011	Test 68, CM-002B
Couch type	Unitized	Foldable	Foldable	Foldable	Foldable	Foldable
Couch-system weight, lb	903.2	886.6	1024.0	957.1	957.1	957.1
Strut stroking distance, in.						
Left foot X-X	3/8	0	1/8	1-1/4	7/8	1-1/4
Right foot X-X	3/8	0	1/4	0	7/8	1-3/8
Left head X-X	1/64	0	0	7-1/4	5-3/8	0
Right head X-X	1/64	0	0	4-1/2	6-3/8	0
Left Z-Z	3-3/4	0	4-1/2	2-1/6	3/8	10-1/8
Right Z-Z	3-5/8	0	4-7/8	0	1-3/4	12-1/16
Left Y-Y	0	0	0	0	0	0
Right Y-Y	0	0	0	0	0	0

TABLE III. - STROKING LOADS OF CREW-COUCH STRUTS

Strut location	Loads, lb											
	Test 16		Test 28		Test 31		Test 63		Test 64		Test 68	
	Design	Actual	Design	Actual	Design	Actual	Design	Actual	Design	Actual	Design	Actual
Left foot X-X	7875	10 600	10 000	6250	6 000	(a)	4960	5200	4960	5700	5975	6950
Right foot X-X	7875	11 500	7 500	4720	4 400	9 670	4230	4950	4230	4400	5316	6100
Left head X-X	5167	3 440	6 000	5400	10 000	4 560	3660	4200	3660	4000	4292	2370
Right head X-X	5167	3 660	4 300	3070	7 500	3 610	3089	4776	3089	4000	3874	3200
Left Z-Z	5171	8 120	10 000	5900	10 000	10 700	3750	4444	3750	3200	5134	(a)
Right Z-Z	5171	7 250	7 400	3820	7 400	5 420	3320	3765	3320	4000	4541	4750
Left Y-Y	8170	0	8 170	0	8 170	300	8170	0	8170	0	8170	4848
Right Y-Y	8170	460	8 170	0	8 170	600	8170	0	8170	0	8170	0

^aBad gage.

TEST INSTRUMENTATION

Photography

Motion picture photography was used extensively to record impact motions during the land-impact-test program. As many as 12 range cameras covered the launching structure and the landing area to record and time the kinematics of the test vehicle. All range cameras operated at 400 frames per second except for the 24-frame-per-second cameras used to document the entire test sequence. The locations and viewing angles of the range cameras for each test are illustrated in appendix A.

Each of the spacecraft structures tested contained a photographic system mounted within the crew compartment. This system recorded the movements of the crew-couch components, anthropomorphic dummies, and vehicle components and equipment. The onboard photographic system usually included five 16-millimeter, high-speed motion picture cameras, a lighting installation, a timing-code complex, a battery power supply, and system control units. In figure 16, the locations of photographic system components within a test vehicle are shown. Films of all impact tests are available at the MSC Film Library.

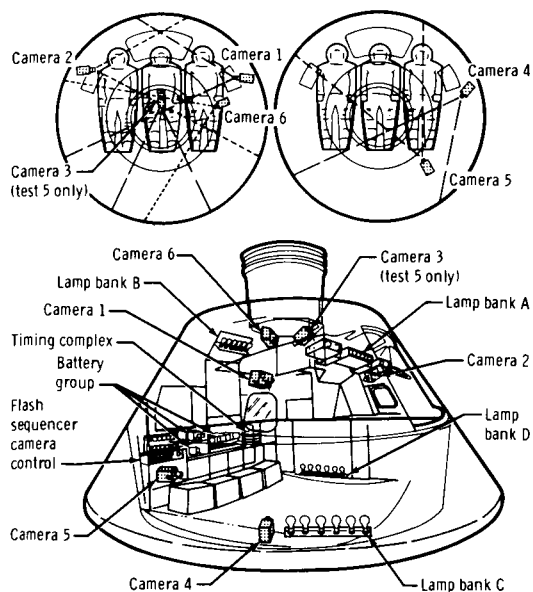


Figure 16. - Photoinstrumentation system in test vehicle.

Instrumentation

Horizontal-velocity measurements of the trolley and the test vehicle were provided by a timing system on the launching structure. A striker in the trolley sequentially broke three carbon electrical conductors mounted on the monorail immediately ahead of the release point of the test vehicle from the trolley. The horizontal release velocity at release was computed from the times of recorded voltage drops caused by breaking the conductors and the known spacings between the conductors.

The level of test-vehicle instrumentation varied from nine channels of data acquisition for the boilerplate tests to as many as 120 channels for the spacecraft tests. Instrumentation of the boilerplate vehicle was limited to range cameras and accelerometers necessary to determine vehicular kinematics and c. g. accelerations. The locations of specific boilerplate instruments are shown in appendix A.

The spacecraft structures and equipment were instrumented with a much greater number and variety of transducers. These included transducers to measure accelerations, strains, and crew-couch-strut deflections. All transducers (except the self-contained instrumentation packages within the crew dummies during tests 16, 28, and 31) were connected to test-facility recording devices by an umbilical cable. Data from accelerometers in the crew dummies during tests 63, 64, and 68 also were recorded through the umbilical cable.

Test-facility recording devices consisted of analog and digital tape recorders. Accelerometer data were recorded on magnetic tape in analog format and later were converted to oscillograms at several frequency filtration levels. Crew-couch-strut loads and deflections also were recorded in analog format and later converted to unfiltered oscillograms. Strain measurements were recorded both in analog and digital format. The analog strain measurements were processed in the same manner as the couch-strut measurements. The digital measurements were processed by computer to produce maximum and minimum normal and shear stresses. Details of test instrumentation including locations and ranges of the various transducers are given in appendix A of this report.

All instrumentation of the test facility and test vehicle, including photographic instrumentation, was centrally timed by an Inter-Range Instrumentation Group B timing track to permit correlation of specific impact events on all transducer recordings.

Accelerations for the first 15 impact tests with boilerplate test vehicles were recorded by the use of a closed-drum oscillograph data-acquisition system. Evaluation of the data revealed that the accelerations were distorted significantly both in magnitude and in wave form by the galvanometers used.

The acceleration data obtained during subsequent boilerplate and spacecraft tests were recorded on magnetic tape and then reproduced on oscillograph machines. These data are presented as unfiltered, filtered at 320 hertz, and filtered at 100 hertz. The filtering process distorts the data by reducing peak values and by introducing a time lag. All acceleration values discussed within this report are the authors' interpretation of the values on unfiltered traces. Interpretation was necessary to distinguish between primary structural accelerations and those accelerations superimposed by high-frequency, low-energy vibrations of specific equipment or instrumentation mountings.

TEST RESULTS

Comparison of the Kennedy Space Center and Manned Spacecraft Center Impact Surfaces

A portable impact test facility was assembled at the MSC to obtain data on the newly constructed impact surface and to verify the new operating procedures. Impact tests were made with BP-25 and BP-1201 at a pitch attitude of -27.5° , a roll attitude of 0° , a horizontal velocity of 37.2 fps, and a vertical velocity of 34.5 fps. The portable test facility then was dismantled and shipped to the KSC where similar tests were conducted near launch pad 39B on the hard-packed fill material.

The test of BP-25 on the MSC impact surface resulted in acceleration peaks of approximately 28g in the X axis and 35g in the Z axis. The same vehicle with the same test parameters produced accelerations at the KSC of 33g in the X axis and 30g in the Z axis. Under similar test conditions at the MSC, BP-1201 was subjected to peak accelerations of approximately 38g in both the X and Z axes. Plots of X axis and Z axis accelerations recorded on BP-25 and BP-1201 during these tests are shown in figure 17. The data reveal that both test vehicles experienced comparable accelerations and that the MSC impact surface closely simulated the KSC pad 39B area in impact characteristics.

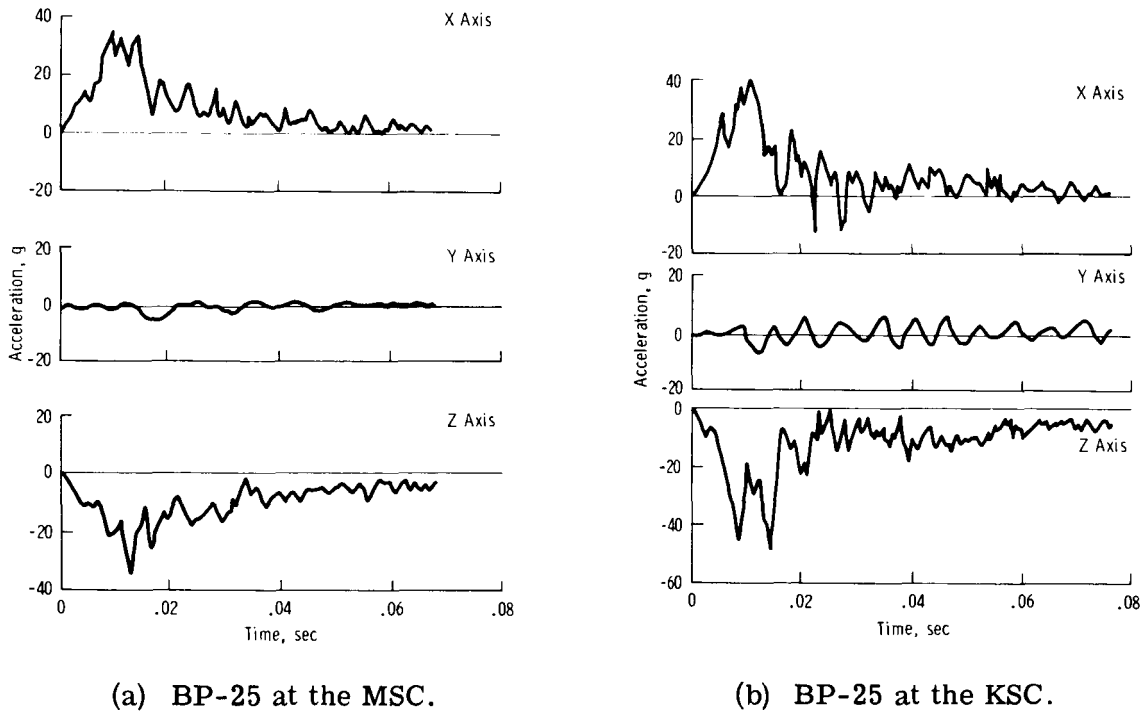
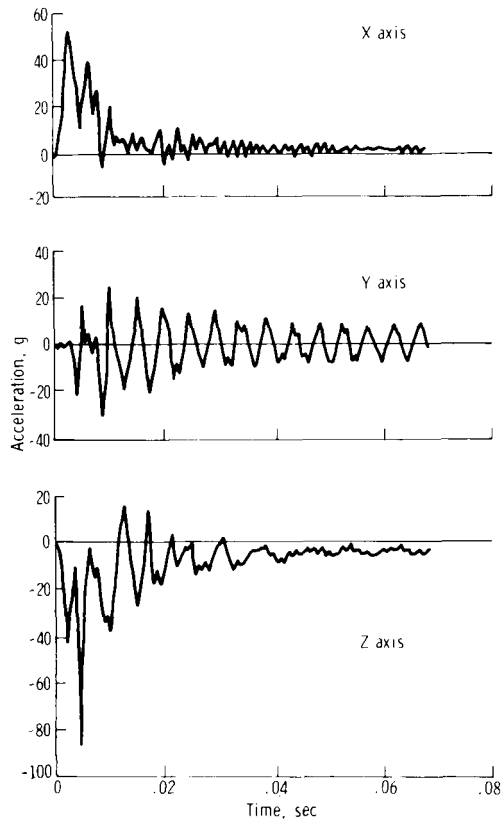


Figure 17. - Boilerplate c. g. accelerations on the KSC and MSC impact surfaces.

Comparison of Kennedy Space Center Terrain Types

A total of 13 impact tests were conducted at the KSC on the six basic types of terrain to determine their relative impact resistance to a landing spacecraft. The test conditions and comparative peak accelerations recorded during each impact test are presented in table IV. In tests 2 to 13 on the other five terrains, the vertical velocity was increased above that used at the MSC and on the KSC fill material. Despite the velocity increase, no significant increases in accelerations were recorded. Thus, a comparison of these accelerations discloses that the fill material of the pad 39B area does produce more severe impacts than the other five terrain types.



(c) BP-1201 at the MSC.

Figure 17. - Concluded.

TABLE IV. - IMPACT-TEST CONDITIONS AND ACCELERATIONS

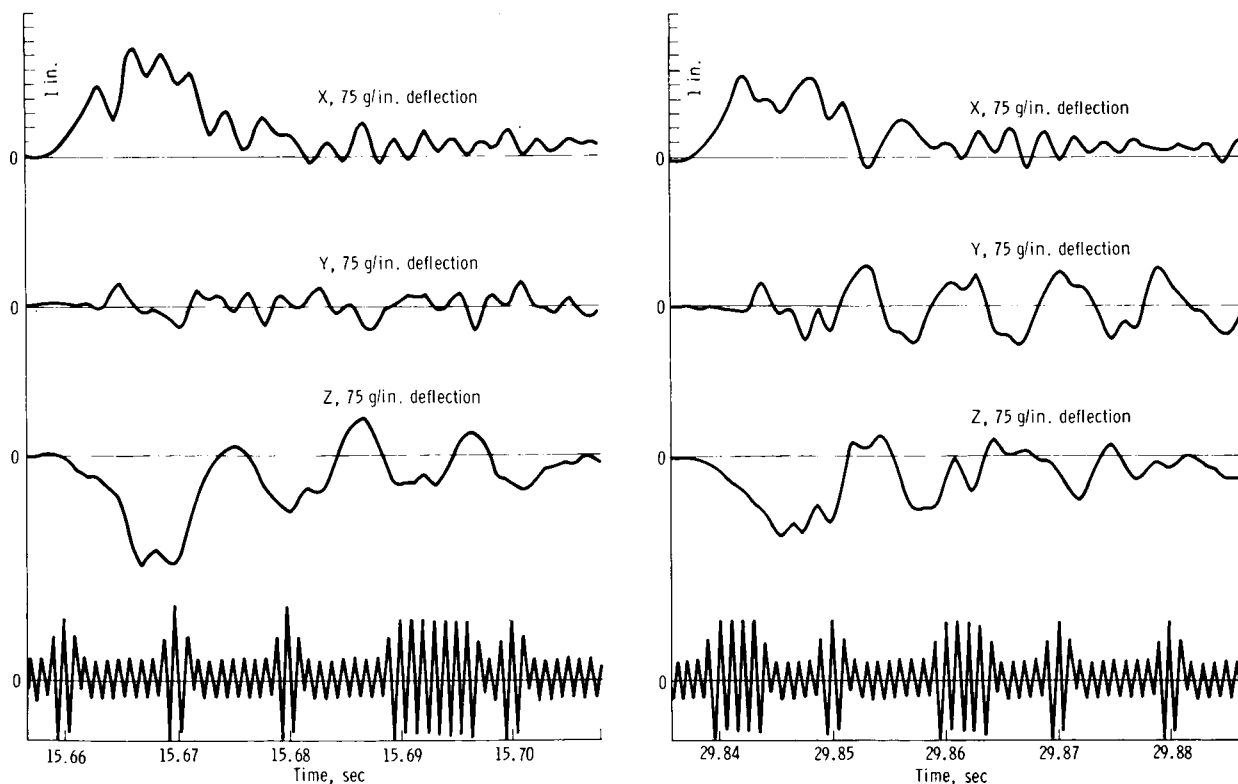
Test location and number	Surface type	Roll, deg	Pitch, deg	Vertical velocity, fps	Horizontal velocity, fps	Peak acceleration at the c. g., g	
						X	Z
MSC	MSC sand	0	-27.5	34.5	38.8	30	28
KSC 1	Pad 39B	0	-27.5	34.5	37.2	35	35
KSC 2	Palmetto	0	-27.5	37.5	36.4	25	28
KSC 3	Palmetto	180	-27.5	37.2	38.8	40	8
KSC 4	Palmetto	0	-36.0	36.9	38.3	18	30
KSC 5	Grass	0	-27.5	39.1	36.5	19	22
KSC 6	Grass	180	-27.5	39.8	37.4	26	12
KSC 7	Grass	0	-36.0	39.0	36.5	23	20
KSC 8	Organic muck	180	-27.5	41.3	37.1	23	8
KSC 9	Organic muck	0	-27.5	41.7	37.9	14	5
KSC 10	Organic muck	0	-36.0	41.8	37.5	5	5
KSC 11	Shallow water	180	-27.5	39.9	38.2	18	6
KSC 12	Shallow water	0	-27.5	39.4	36.1	8	5
KSC 13	Shallow water	0	-36.0	39.5	36.3	7	3

Manned Spacecraft Center Test Program

A total of 47 boilerplate land-impact tests were conducted at the MSC test facility to obtain inexpensively as much parametric data as possible within a short time. A complete tabulation of all test conditions is included in appendix B. The boilerplate structures produced acceleration and kinematic data that could be compared with data obtained with spacecraft structures. This approach was an economical means of predicting reactions of the more costly spacecraft structures.

A total of five spacecraft vehicles (six tests) was impacted to verify the boilerplate results and to establish the land-landing capability of flight-type structures. The impact tests with boilerplate and spacecraft vehicles could be divided into three basic groups: 0° roll landings, 180° roll landings, and skewed landings (where the direction of travel does not coincide with the X-Z plane). Pitch attitudes were varied between -18° and -36° to simulate a range of possible impact attitudes resulting from the parachute rigging tolerances and from the swinging motion of a CM descending under a parachute cluster. All spacecraft tests were conducted at a vertical velocity of 32 fps to simulate the nominal descent rate with three deployed parachutes because a two-parachute recovery terminating in a land landing would be the result of a double system failure.

Ten tests were conducted at a vertical velocity of 38 fps to determine the magnitudes of the accelerations should one of the three parachutes fail to deploy. In figure 18, the effects of vertical velocity on acceleration are shown. This figure contains the X,



(a) Vertical velocity of 38 fps in test 81.

(b) Vertical velocity of 32 fps in test 80.

Figure 18. - Center-of-gravity accelerations from 38-fps and 32-fps vertical velocities.

Y, and Z axis accelerations recorded during two boilerplate tests in which the rate of descent at impact was 38 and 32 fps. There was no horizontal velocity, and the initial pitch attitude was maintained at -27.5° during each test. The peak c. g. accelerations increased from approximately 42g to 52g in the X axis and from 37.5g to 52.5g in the Z axis. The kinetic energy expended during the 32-fps test was 780 000 foot-pounds compared with 1 100 000 foot-pounds during the 38-fps test. The difference represents an increase in energy of 40.8 percent. This significant increase in acceleration and kinetic energy is estimated to exceed the structural capability of the command module.

Tests at 0° Roll

Earlier tests with models and full-scale boilerplates indicated that the most severe accelerations during land landings occurred when the test vehicle impacted at a roll orientation of 0° . Fourteen boilerplate and two spacecraft tests were conducted to define the capability of the CM to withstand the 0° roll landing.

The kinematics resulting from all 0° roll landing tests were similar. The test vehicle impacted on the +Z axis of the aft heat shield with a horizontal velocity vector approximately parallel to and in the direction of the Z axis. The +Z edge of the aft heat shield penetrated the soil to a maximum depth of approximately 7-5/8 inches and then slid forward with the bottom section of the heat shield plowing a shallow furrow. The pitch attitude trimmed from -27.5° to approximately -10° , an attitude change of only 17° . The slide-out distance increased slightly with increases in horizontal velocity. When impacted with a horizontal velocity of 25 fps, the vehicle slid approximately 3 feet. An increase in horizontal velocity to 43.5 fps increased the slide-out distance to approximately 5 feet. During tests in which the vehicle landed with a horizontal velocity of 54 fps, the slide-out distances were approximately 9 feet. The kinematics typical of these tests are pictured in figure 19.

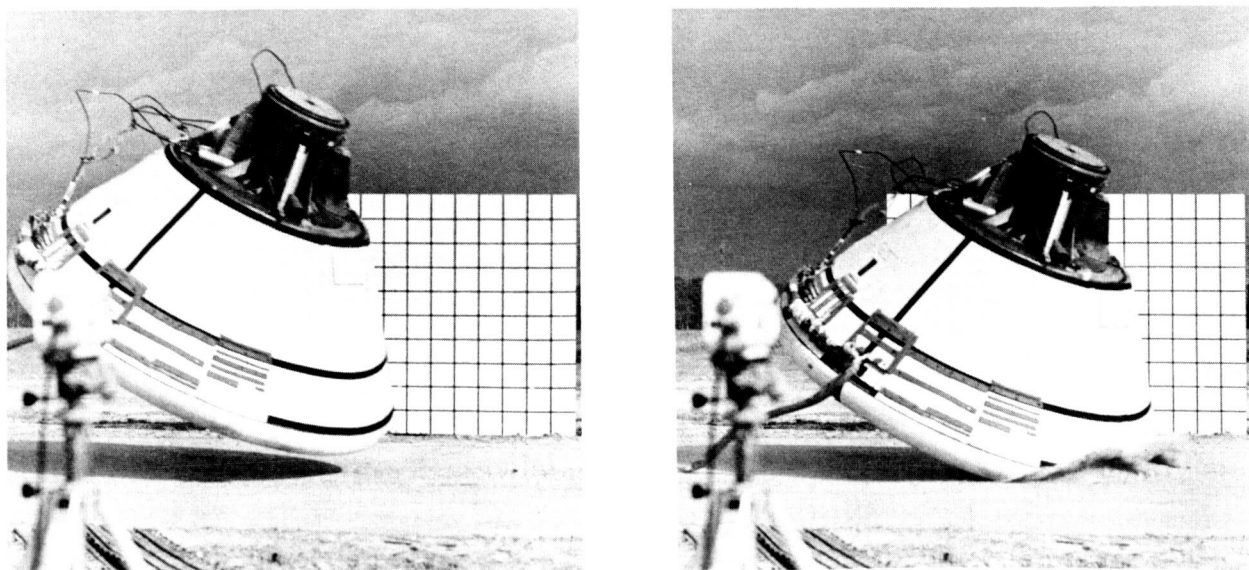


Figure 19. - Landing dynamics during a 0° roll test.

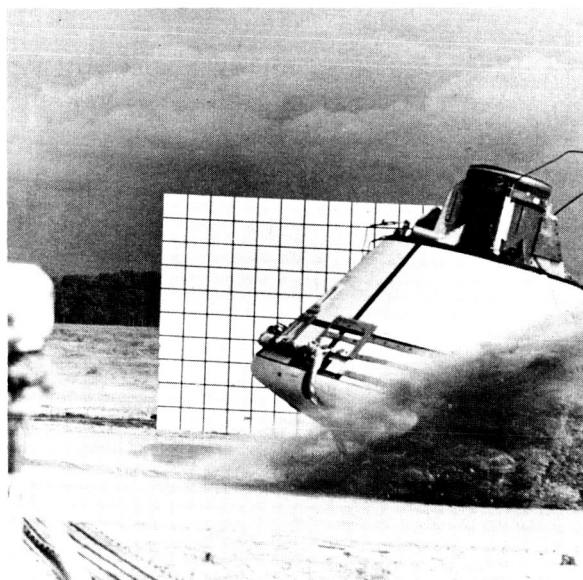
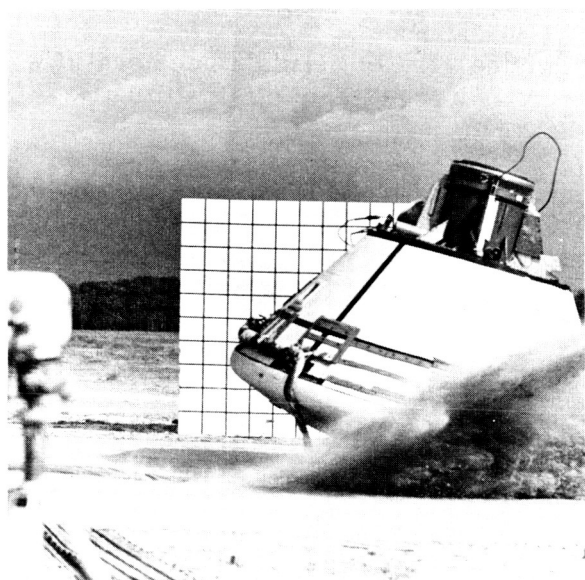
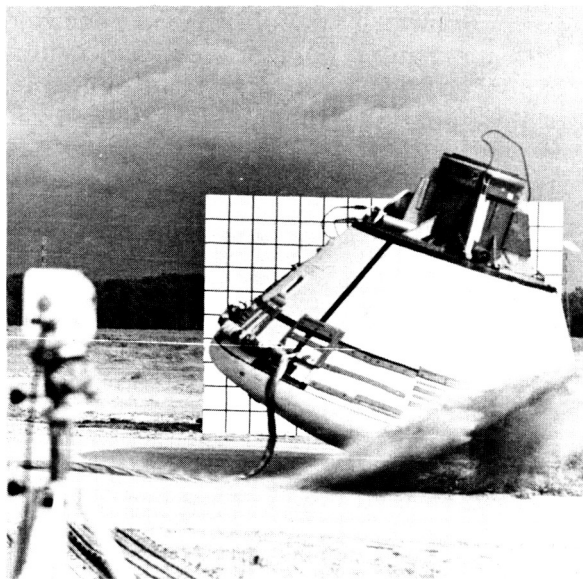
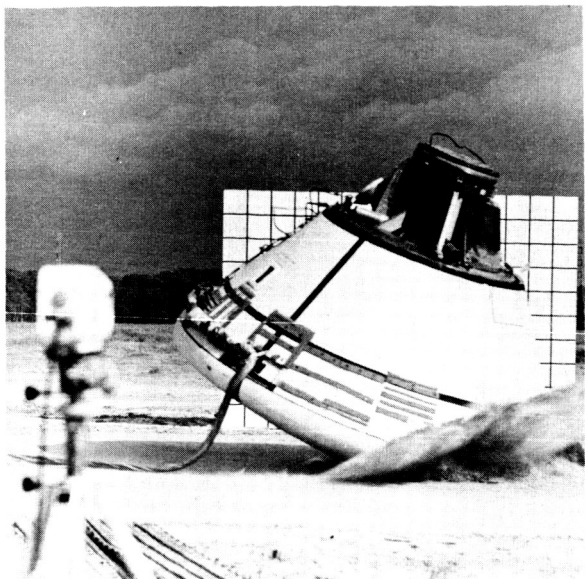


Figure 19. - Concluded.

Roll tests were conducted at 0° with BP-1201 at pitch attitudes of -18° , -27.5° , and -36° to evaluate the effect of pitch-angle variation on stability and accelerations. All 0° roll tests conducted with pitch angles smaller than -27.5° produced stable landings during impact. However, when the pitch angle was increased to -36° and the horizontal velocity was increased to 54 fps, the vehicle (BP-1201) penetrated the impact surface to a depth sufficient to produce a high horizontal force and turned over slowly, impacting again on the +Z sidewall.

Peak c. g. accelerations recorded during the BP-1201 tests generally decreased with increasing horizontal velocities and pitch attitudes because more of the energy was expended through sliding friction and soil penetration by the sharper entrance attitude of the vehicle. These relationships are shown in the plots of figures 20 and 21.

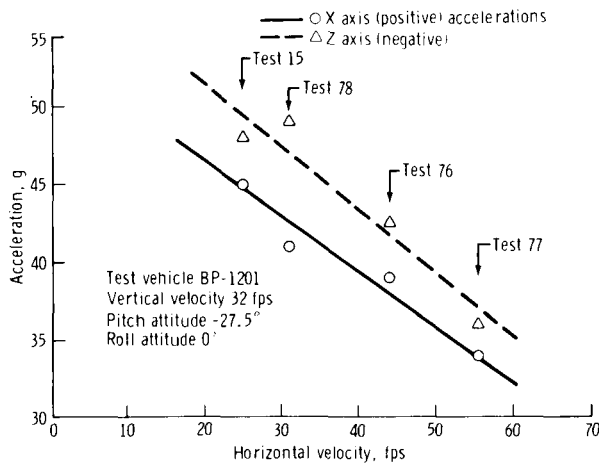


Figure 20. - Boilerplate accelerations as a function of horizontal velocity.

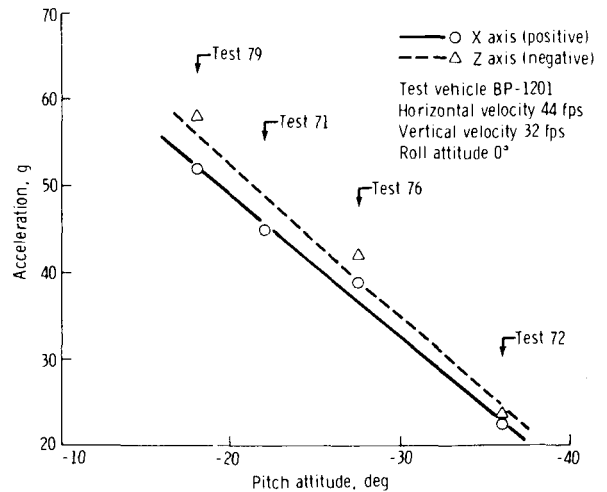


Figure 21. - Boilerplate accelerations as a function of pitch attitude.

The boilerplate tests accurately predicted spacecraft accelerations. The boilerplate test data indicate (fig. 20) that at a horizontal velocity of 25 fps and the nominal pitch attitude of -27.5° , the peak c. g. acceleration would be approximately 45g in the X axis and 47g in the Z axis. When BP-28A was tested under the same impact conditions, peak c. g. accelerations were 43.5g in the X axis and 45g in the Z axis.

An increase in horizontal velocity to 43.5 fps with BP-1201 resulted in peak c. g. accelerations of 39.5g in the X axis and 42.5g in the Z axis. When CM-009 was impact tested at the same impact conditions, 37g in the X axis and 45g in the Z axis were experienced. The X axis and Z axis peak c. g. accelerations recorded during tests of BP-28A and CM-009 are plotted in figure 22 as functions of horizontal velocity. The boilerplate data plot is also included in this figure. Assuming that a gross structural failure does not occur and that the same general relationship between horizontal velocity and accelerations found for BP-1201 (fig. 20) also applies to spacecraft, an increase to 54 fps

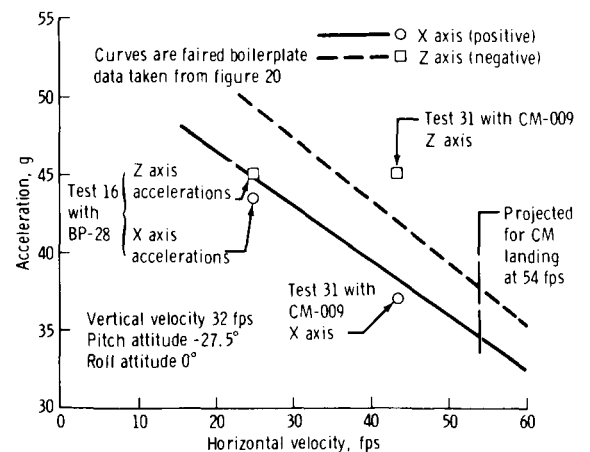


Figure 22. - Comparison of spacecraft and boilerplate accelerations.

in the horizontal landing velocity of a spacecraft would result in X axis and Z axis peak c.g. accelerations of 30g and 38g, respectively. This extrapolation is shown in figure 22.

The acceleration experienced during a 0° roll landing is a single pulse of approximately 0.045-second duration with principal components being in the X-Z plane. The X axis and Z axis accelerations recorded during impact tests of BP-28A and CM-009 are shown in figures 23 and 24.

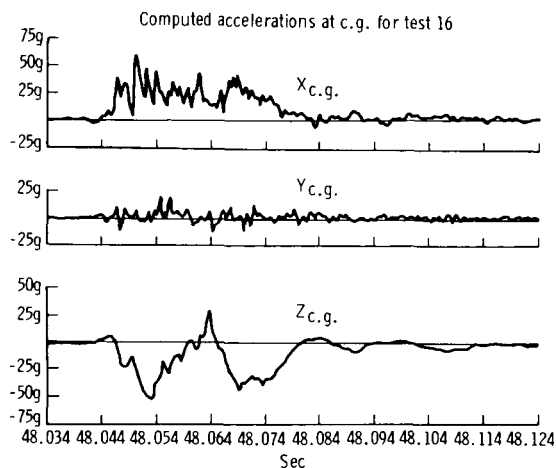


Figure 23. - Accelerations from test 16 with BP-28A.

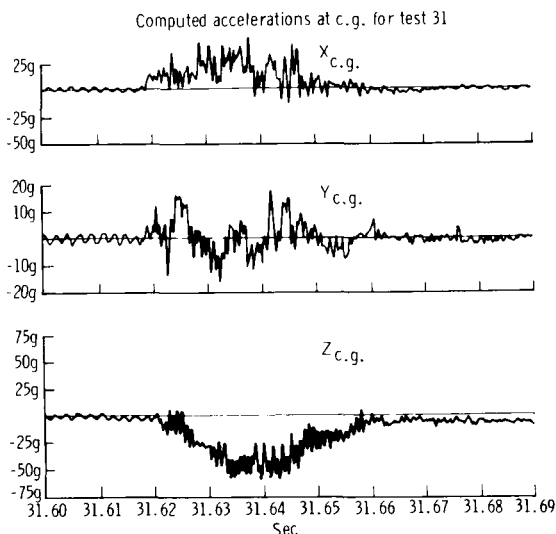


Figure 24. - Accelerations from test 31 with CM-009.

Damage to spacecraft structures caused by 0° roll landings was less extensive than had been expected. The damage was limited largely to the +Z area of the aft bulkhead, heat shield, and crew-compartment sidewall. The aft heat shield was crushed into the aft equipment bay, causing damage to the RCS oxidizer tanks and related equipment installed in that area. Frames and cores were crushed, fractured, and debonded from the sidewall throughout a sector of approximately 60° . Several face-sheet cracks and separations occurred in the honeycomb core of the crew-compartment sidewall. These openings could admit toxic fumes from the ruptured RCS tanks into the crew compartment. Apparently, no other failures occurred either in primary structure or in secondary equipment. The primary damage sustained during the impact test of CM-009 (typical of the 0° roll landing damage) is shown in figure 25.

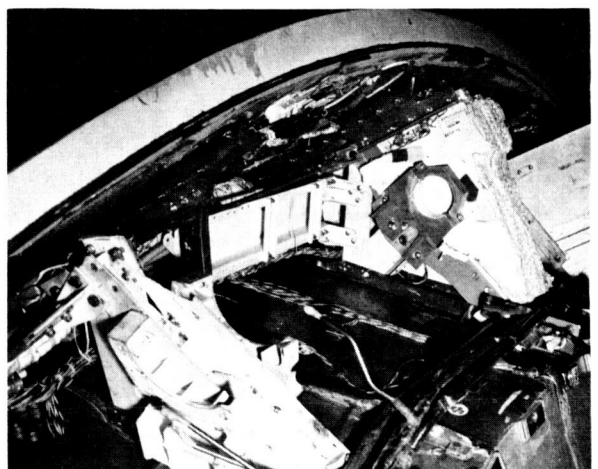
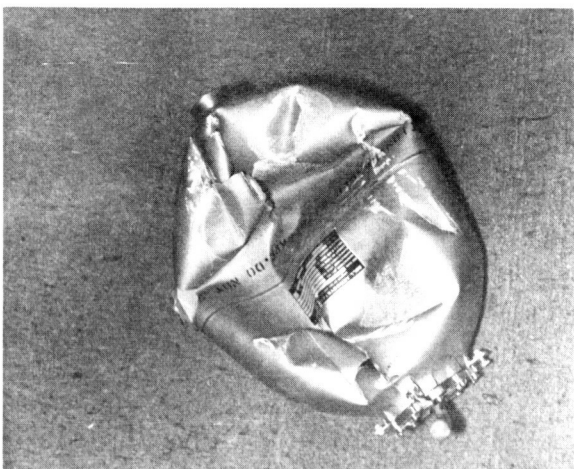
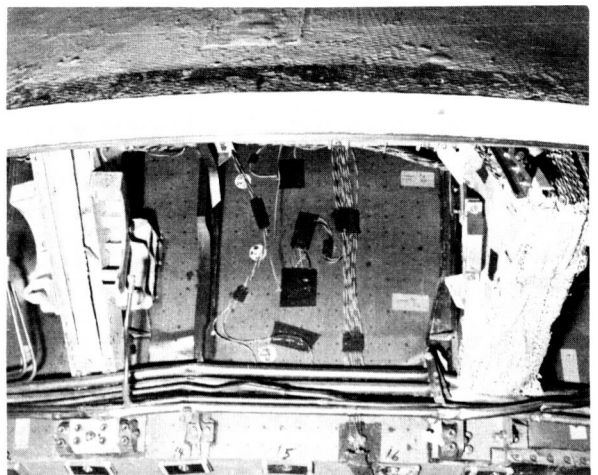
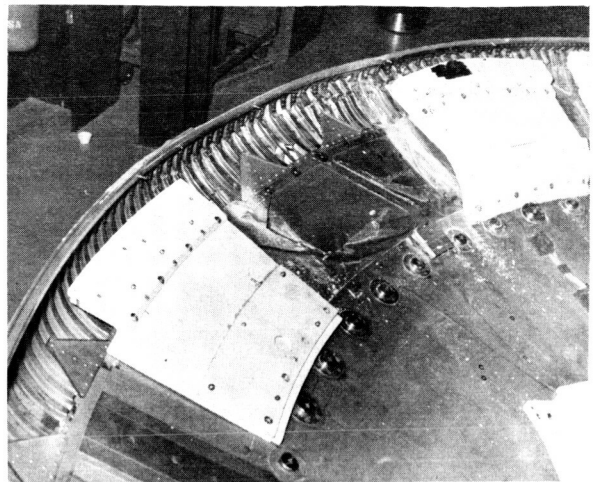
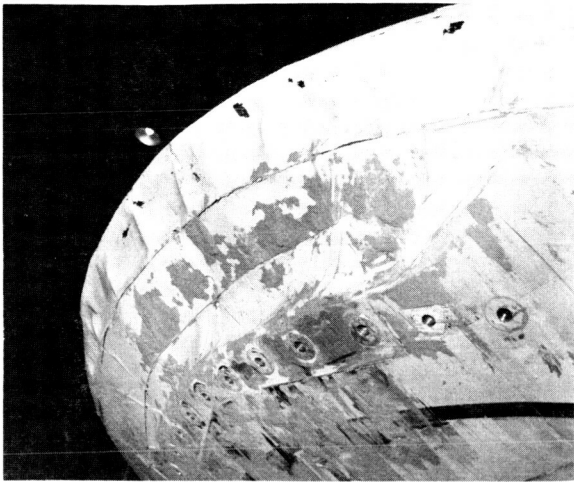


Figure 25. - Impact damage to CM-009 in test 31.

Tests at 180° Roll

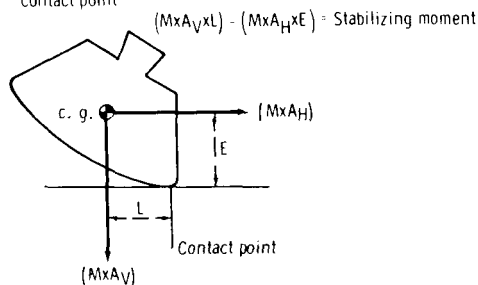
Thirteen tests with BP-1201 and spacecraft tests with CM-008, CM-009, and CM-011 were conducted to define the capability of the Apollo CM to withstand 180° roll landings. Unlike the 0° roll tests, all landings at a roll of 180° were unstable, even at relatively low horizontal velocities (25 fps). As the horizontal velocity was increased, the tumbling of the test vehicle became more violent because of the spherical shape of the heat shield and the direction of the forces involved.

The direction of the inertial forces that act upon a vehicle during 0° and 180° roll landings are shown in figure 26. During a 0° roll landing, the overturning or destabilizing moment about the contact point produced by the horizontal inertial force is opposed by the moment produced by the vertical inertial force. Therefore, the vehicle is inherently more stable in a 0° roll orientation. The process can be expressed by the following simple summation of resulting moments for 0° roll case.

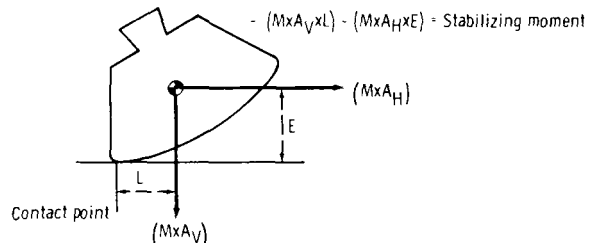
$$(M)(A_V)(L) - (M)(A_H)(E) = \text{Stabilizing moment}$$

where A_V and A_H are vertical and horizontal accelerations of the c.g., M is the mass of the vehicle, L is the horizontal moment arm from the contact point to the c.g., and E is the vertical moment arm from the contact point to the c.g. Apparently, the vertical inertial force adds to the stability of the system in a 0° roll landing (fig. 26(a)).

- M = mass of vehicle
- c.g. = center of gravity
- A_H = horizontal acceleration
- A_V = vertical acceleration
- E = height of c.g. above contact point
- L = horizontal displacement of c.g. from contact point



(a) Landing at 0° roll.



(b) Landing at 180° roll.

Figure 26. - Factors in the dynamics of a CM landing.

When the direction of travel is reversed, as in 180° roll landings, the two moments (of the previous equation) become additive, producing a high angular acceleration about the c.g. of the vehicle. This high angular acceleration results in a violent rotation of the vehicle about its aft heat shield. As the vehicle rotates from a negative pitch attitude through 0° , an upward acceleration is imparted to the c.g., as shown in figure 27. When the surface contact point reaches the $-Z$ edge of the aft heat shield (at a pitch of approximately 30°), the vertical velocity causes the vehicle to leave the impact surface with a trajectory angle of approximately 50° from the horizontal and to continue to rotate and translate in free flight until another impact occurs.

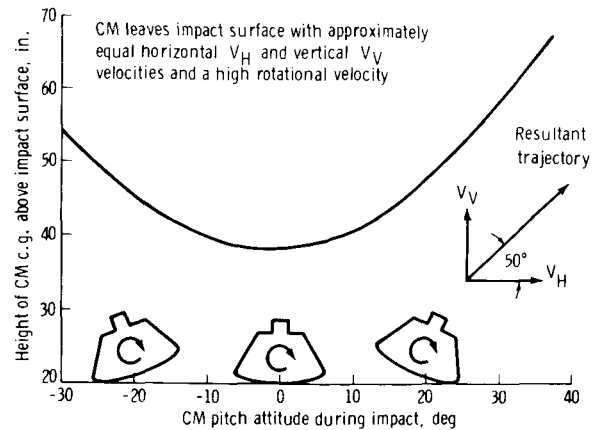


Figure 27. - Theoretical trajectory of CM c.g. during a 180° roll impact.

Because much of the initial horizontal velocity of the test vehicle was converted into upward thrust, the attitude and velocity of the vehicle at second impact was highly sensitive to changes in the initial horizontal velocity. A variety of impact attitudes was possible for the second impact, and it was necessary to select specific test conditions that would load critical structural areas. The boilerplate vehicle constituted an inexpensive tool for the prediction of secondary impact conditions. Boilerplate tests revealed that at horizontal velocities of approximately 25 fps, the test vehicle would overturn and impact on the $-Z$ side of the upper deck and docking tunnel. As the horizontal velocity was increased to 43.5 fps, the vehicle rotated about 300° and impacted on the lower $+Z$ sidewall. As the horizontal velocity was increased to 54 fps, the vehicle impact rotated approximately 360° and reimpacted on the aft heat shield.

Conditions were selected for the test of CM-008 to assess the damage to the upper deck and docking tunnel should the second impact of a land landing occur on this area. The test conditions to achieve such an attitude at second impact included a roll of 180° , a pitch of -27.5° , and a horizontal velocity at initial impact of 25 fps. The kinematics of the test of CM-008 are shown in the photographic sequence of figure 28. The upper deck, the docking tunnel, and the $+Z$ sidewall of the crew compartment were damaged extensively (fig. 29). Many fractures occurred in the structures of the docking tunnel and upper deck, and extensive debonding of the main-display-panel support occurred. However, all damaged members remained attached to the structure of the test vehicle and did not present a significant crew hazard. The aft bulkhead was buckled approximately 6 to 8 inches into the crew compartment by the aft heat shield, and the crew-compartment sidewall was cracked completely through its core on the $+Z$ side. The initial impact conditions for test 63 (second test of CM-009) were selected to determine the effects of a secondary impact on the $+Z$ sidewall.

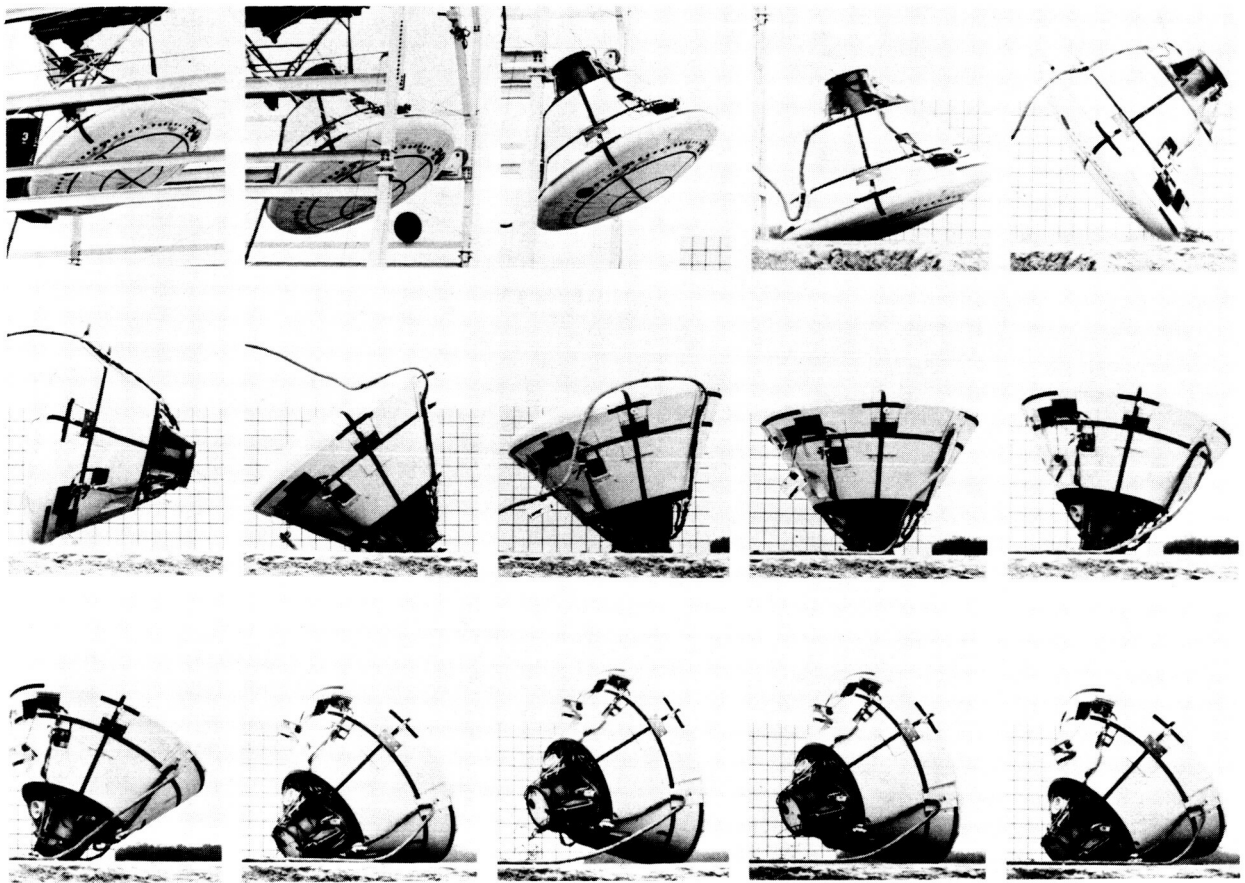


Figure 28. - Landing dynamics of CM-008 during test 28.

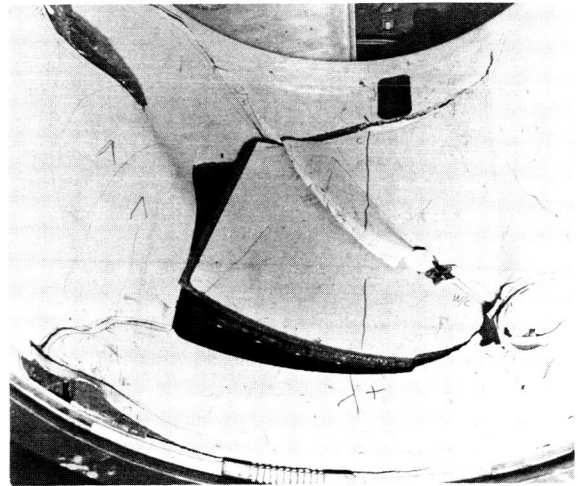
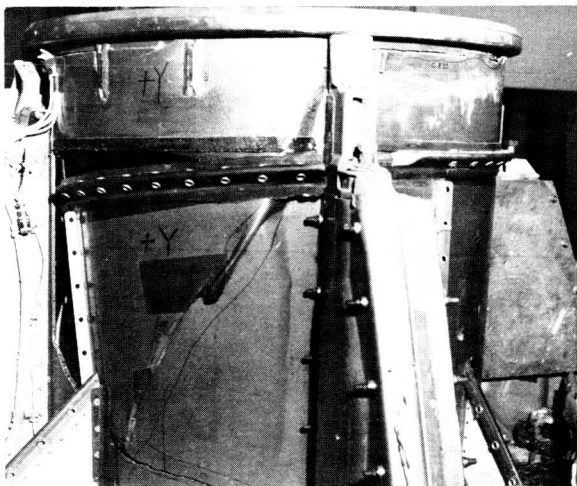


Figure 29. - Impact damage to CM-008.

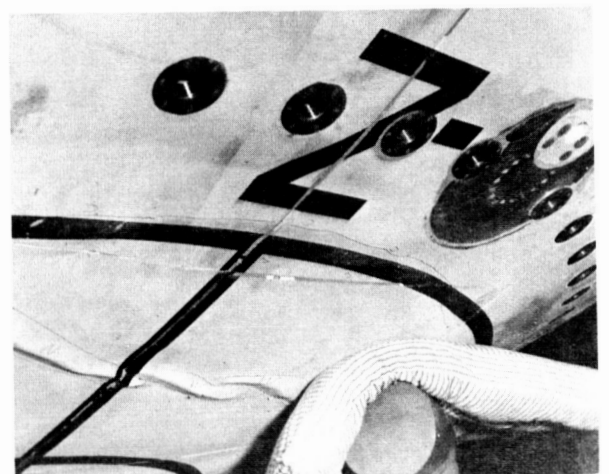
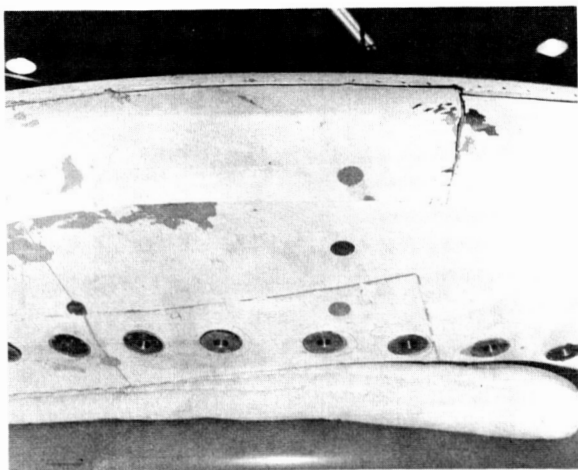
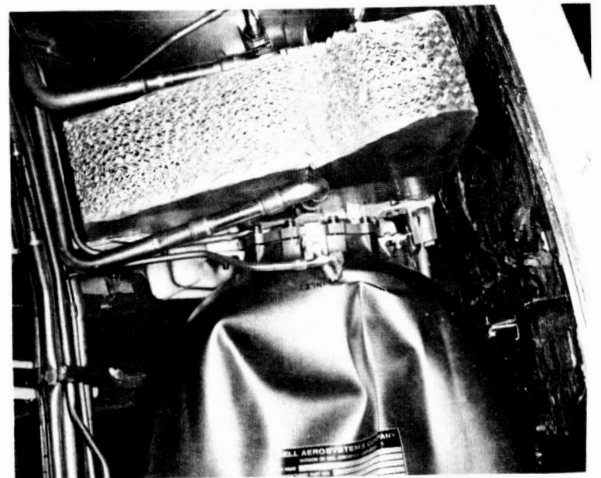
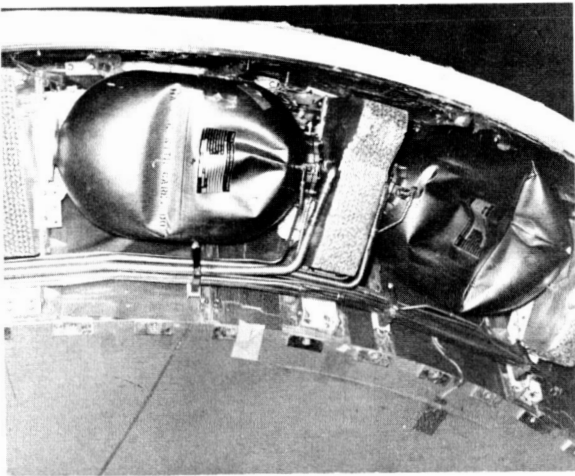
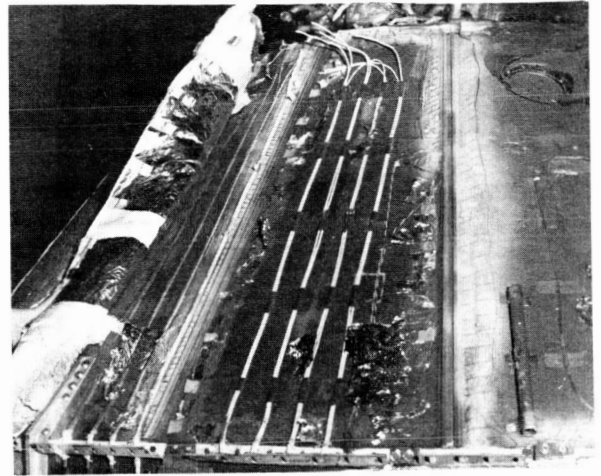
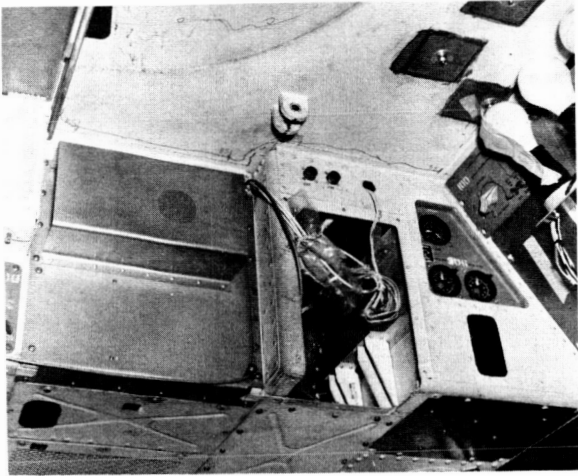


Figure 29. - Concluded.

The impact test of CM-009 at 180° roll and 43.5 fps horizontal velocity produced more violent impacts than those of the CM-008 test. The rotation during the landing of CM-009 in test 63 is pictured in figure 30. The damage to the structure of the test vehicle in test 63 was more extensive than in any previous test. Damage to the docking tunnel and forward bulkhead was light, but significant damage occurred to the aft heat shield, aft bulkhead, and crew-compartment sidewall.

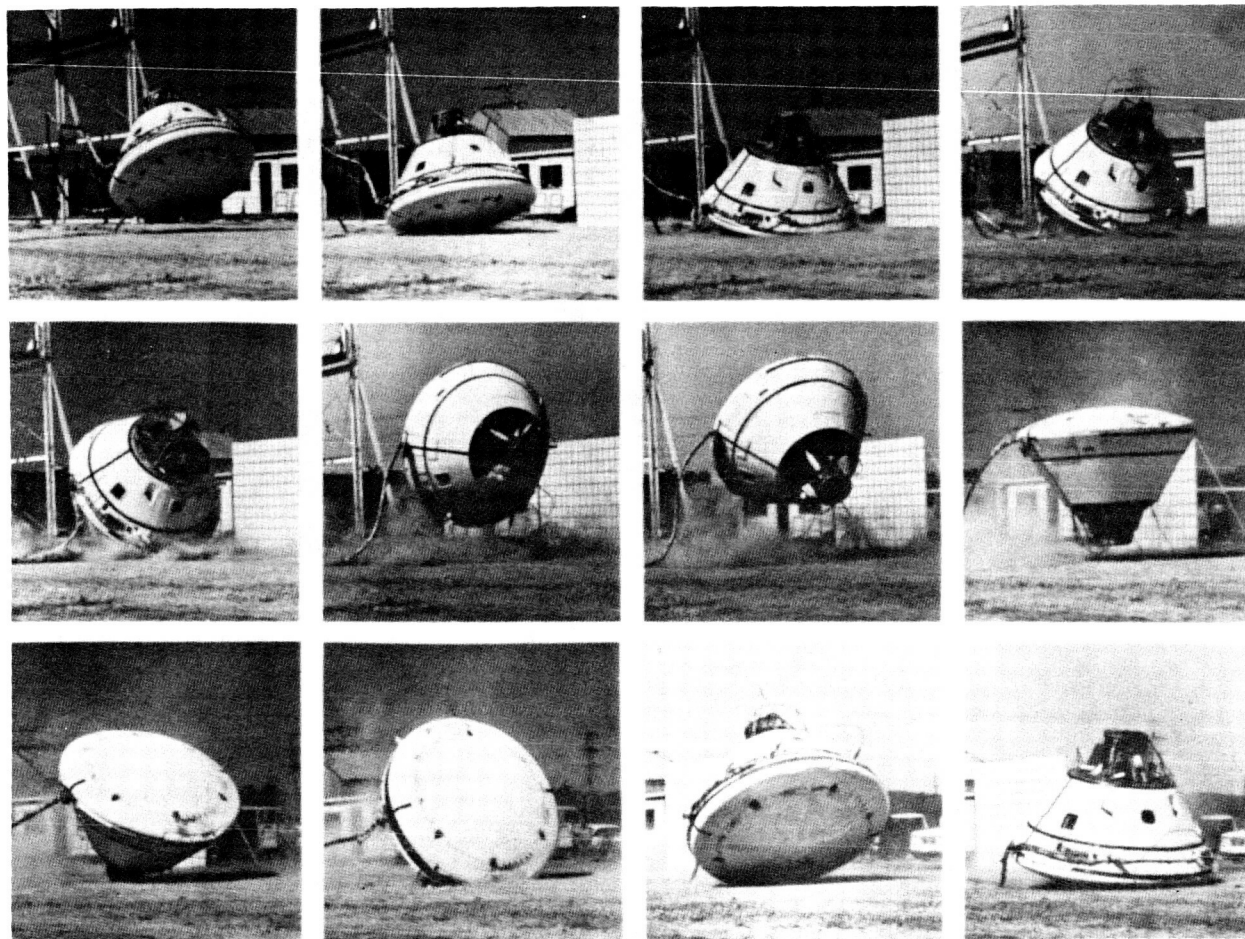
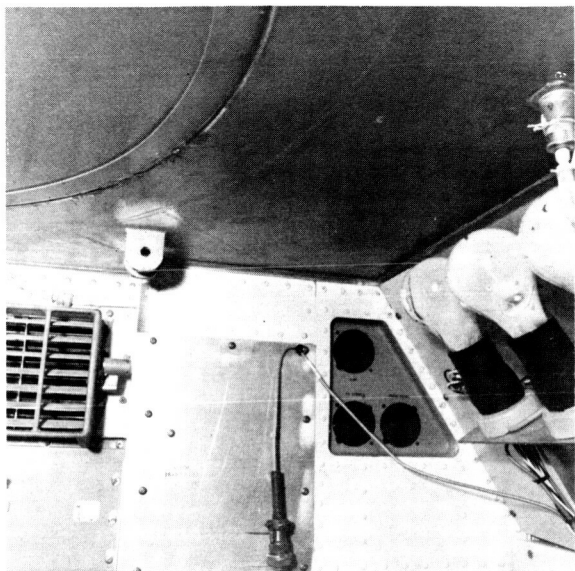


Figure 30. - Landing dynamics of CM-009 during test 63.

Although the docking tunnel contacted the impact surface on the +Z sector, the loading was light and no damage occurred to the tunnel. Debonding occurred between the forward bulkhead and the sidewall on the +Z side (fig. 31(a)), but no debonding occurred on the main display console.

The crew-compartment sidewall between stations $X_c = 42.0$ and $X_c = 81.5$ on the +Z side was crushed inward by the crew-compartment heat shield (fig. 31(b)). Several large cracks occurred through the +Z sector of the sidewall behind the lower equipment bay (fig. 31(c)), and the entire lower equipment bay was debonded from the

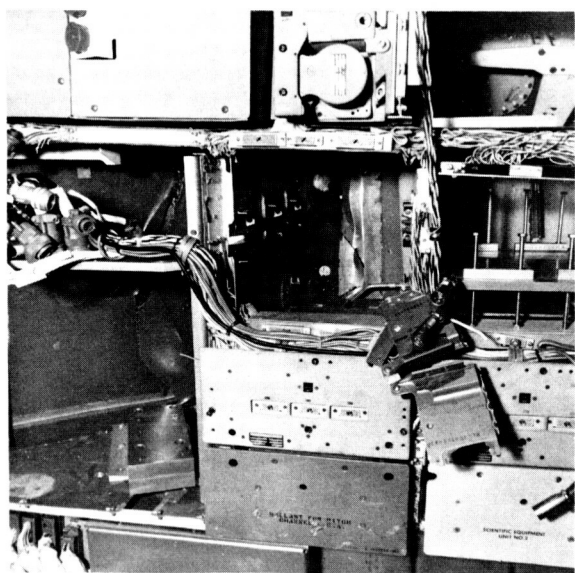
sidewall, which caused the equipment shelves to deflect under their own weight approximately 2 inches. Although extensive damage occurred on the sidewall in the oxygen surge tank area (fig. 31(d)), the surge tank was not damaged.



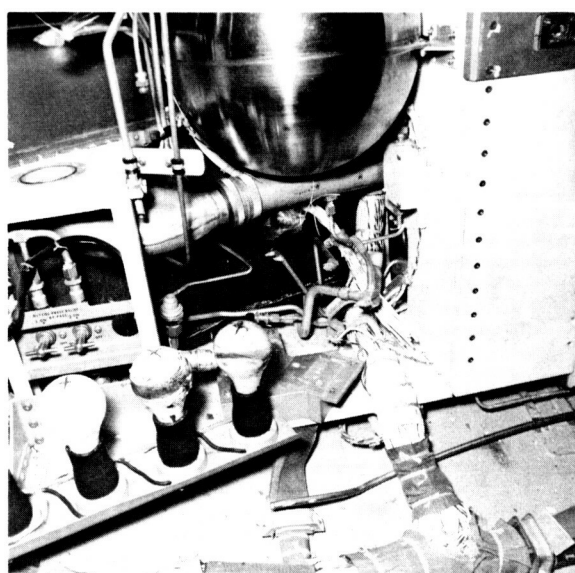
(a)



(b)



(c)

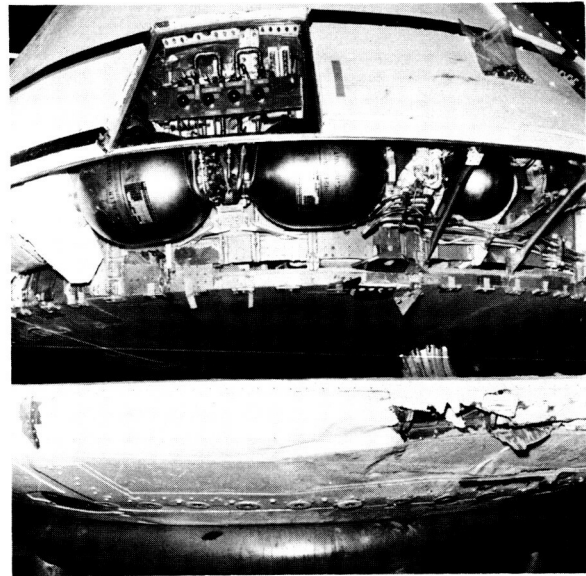


(d)

Figure 31. - Damage to CM-009 during a 180° roll landing.



(e)



(f)

Figure 31.- Concluded.

The aft-bulkhead core failed in shear in an area approximately 6 feet in diameter in the +Z sector, and a crack through both face sheets extended approximately 36 inches from the center in the +Z direction (fig. 31(e)). The oxidizer tanks were crushed, and the fluid from the tanks escaped and entered the crew compartment through the crack in the aft bulkhead. The aft bulkhead was separated from the crew-compartment sidewall through an included angle of 196° (fig. 31(f)).

Test 64 with CM-011 was conducted at a horizontal velocity of 54 fps, equivalent to the maximum wind velocity in which the launch vehicle can be operated. The resulting kinematics were even more violent than those of test 63 with CM-009. The second impact of CM-011 occurred at a pitch attitude of approximately 300° and loaded the aft sidewall and heat shield more severely in the X axis direction and less in the Z axis direction than did the test conditions of CM-009. The aft area of CM-011 was damaged to a greater extent than that of CM-009. However, the separation of the aft bulkhead from the aft sidewall was less extensive, occurring throughout a 110° segment of the sidewall. The damage included numerous cracks in the aft bulkhead and sidewall that could permit the passage of toxic fumes and fluids from the aft equipment bay. On second impact, the sidewall beneath the crew hatch was crushed inward and upward from 12 to 18 inches, which fully compressed the Z-Z struts of the crew couch and produced high accelerations in the crew-couch system. The kinematics of the CM-011 test are shown in figure 32, and typical damage is pictured in figure 33.

Slight variations occurred in the impact kinematics between spacecraft tests 63 (CM-009) and 64 (CM-011) and similar tests of BP-1201. Essentially, the boilerplate vehicle was a rigid body. In contrast, the structure of the spacecraft yielded and absorbed a considerable amount of the impact energy. Furthermore, this deformation of the spacecraft changed the shape of the heat-shield surface about which the vehicle rotated before second impact.

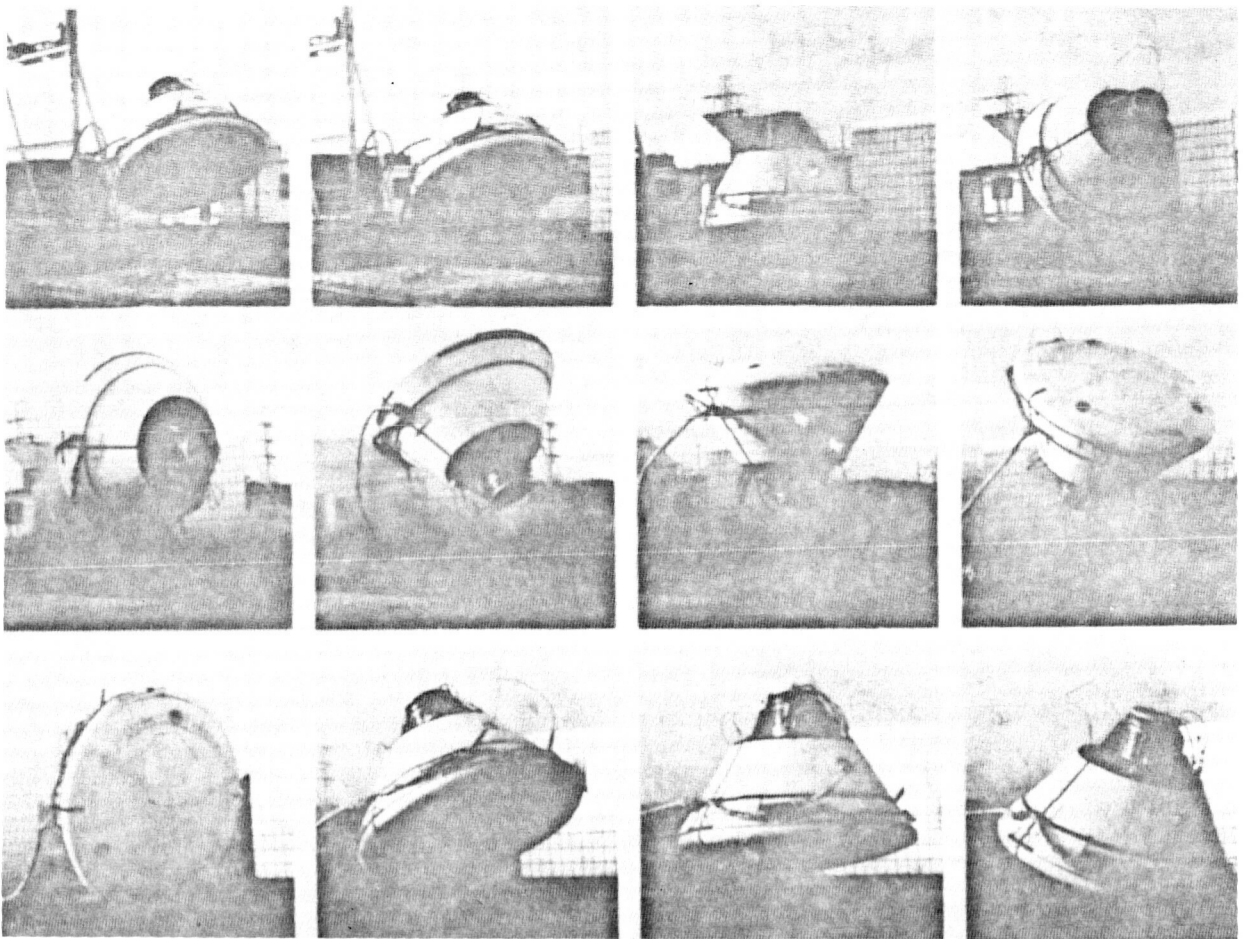


Figure 32. - Landing dynamics of CM-011 during test 64.

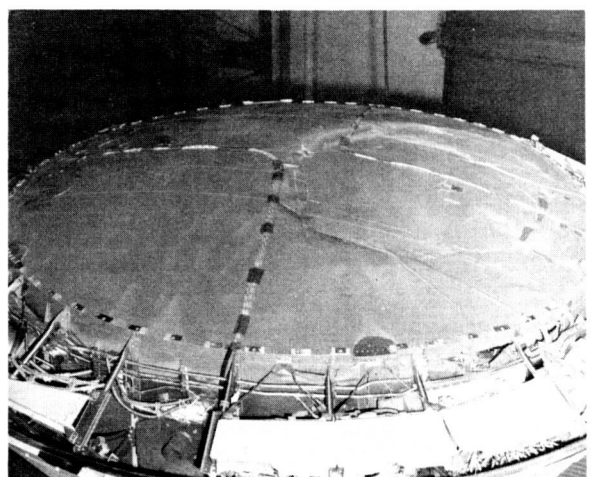
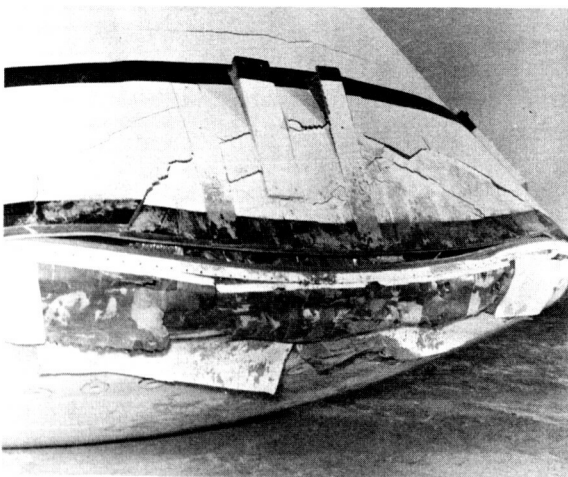


Figure 33. - Impact damage to CM-011.

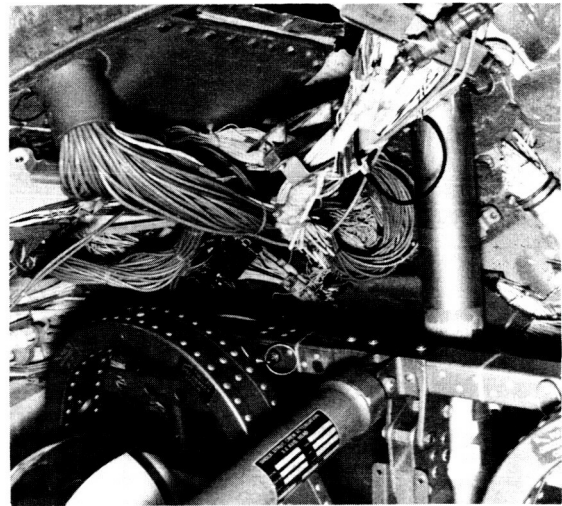
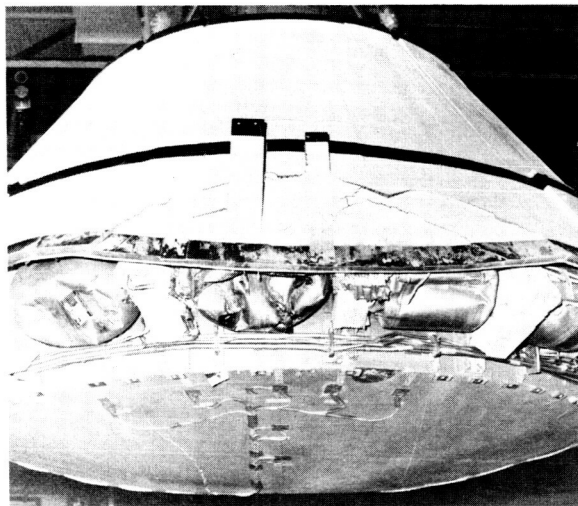
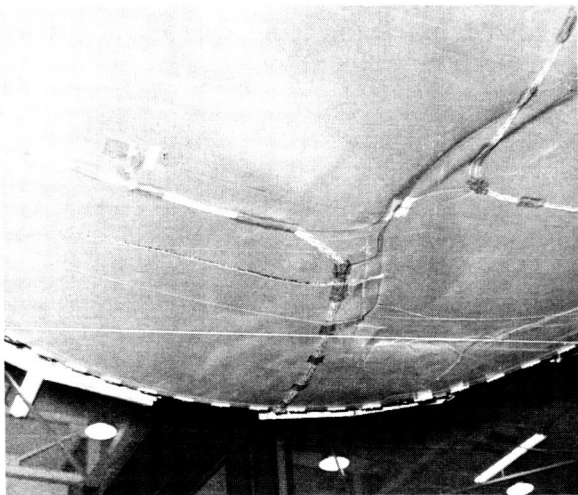


Figure 33. - Concluded.

The accelerations recorded during the initial impacts of 180° roll tests displayed a characteristic shape regardless of the initial horizontal velocity. The X axis and Z axis accelerations at the c. g. of the three tested spacecraft and the three corresponding boilerplate tests are presented in figures 34 to 39. The six figures indicate that significant X axis peak accelerations occurred during the first 0.02 second of impact and varied from 33g to 45g for the spacecraft and from 40g to 50g for the boilerplate vehicle. A second, relatively high, acceleration spike of 20g and 30g occurred approximately 0.1 second later as the test vehicle rolled past the center of its heat shield. The velocity vector of the c. g. was toward the ground as the vehicle rolled about the heat shield from a pitch attitude of -27.5° to approximately -2° . As the vehicle rotated through 0° pitch, the rotation accelerated the c. g. upward significantly in the direction of the X axis. The acceleration along the Z axis at the c. g. was almost insignificant because of the more gradual velocity changes in that direction. The X axis c. g. velocity vector underwent a direction change of 180° in a few milliseconds. The highest

Z axis c.g. accelerations occurred during the second impact and ranged from 20g to 30g for the spacecraft and 30g to 35g for the boilerplate vehicle.

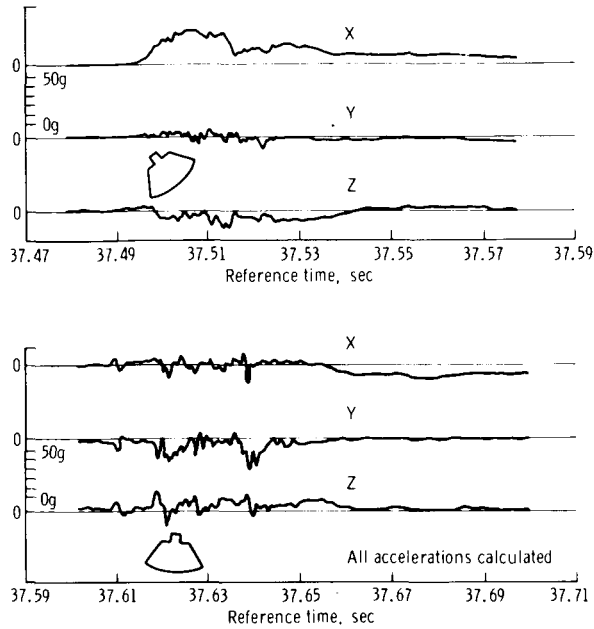


Figure 34. - Accelerations at c.g. recorded during test 28 with CM-008.

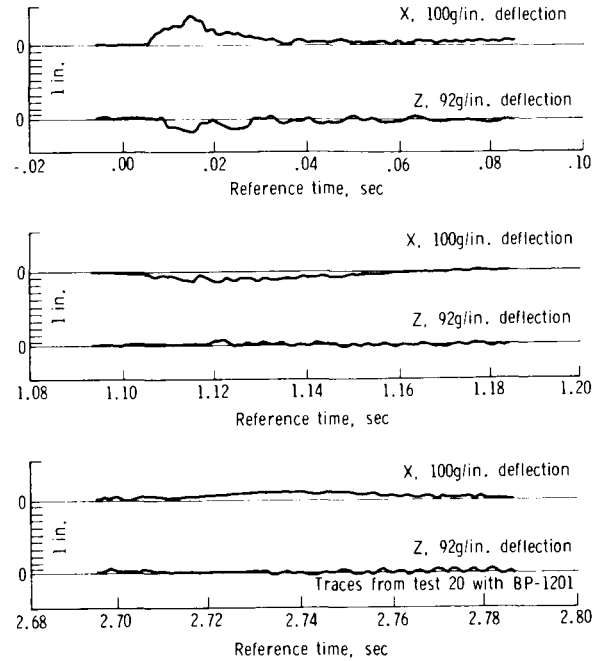


Figure 35. - Boilerplate c.g. accelerations under conditions of test 28.

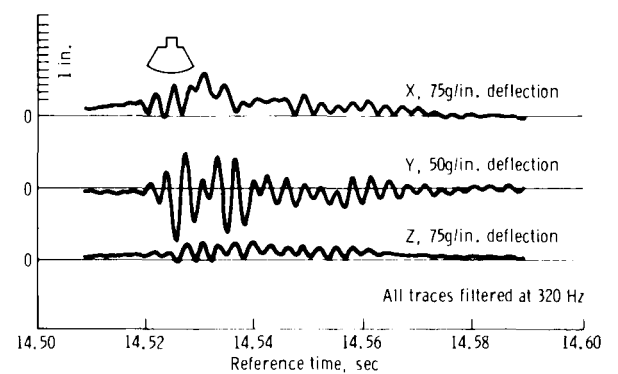
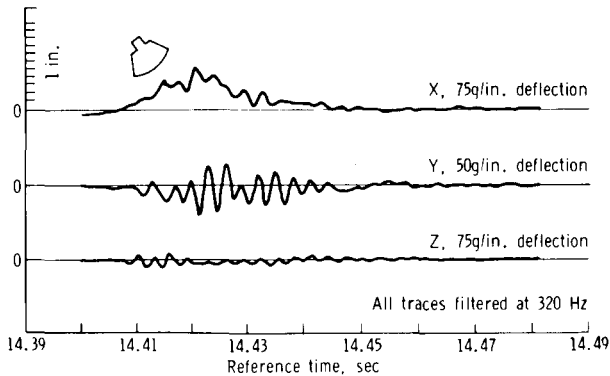


Figure 36. - Accelerations at c.g. during test 63 with CM-009.

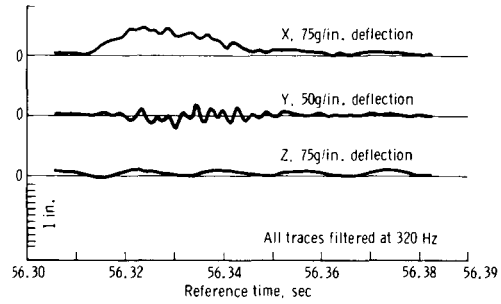
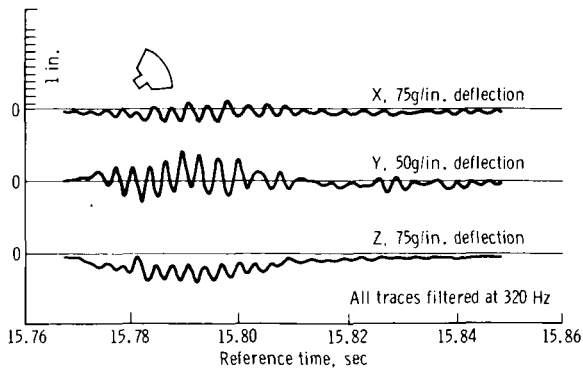


Figure 36. - Concluded.

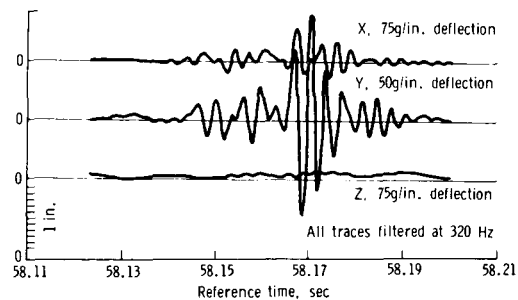
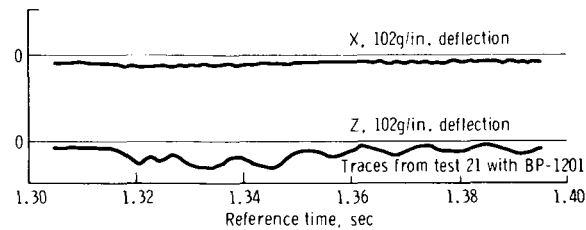
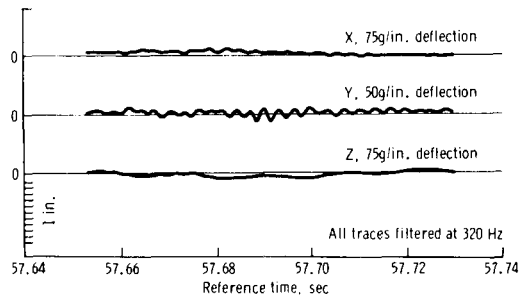
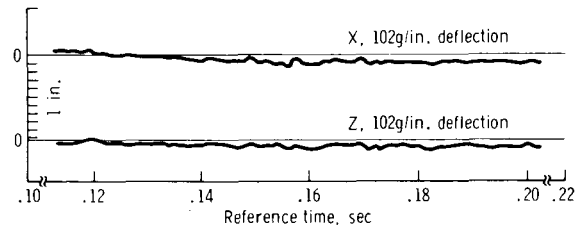
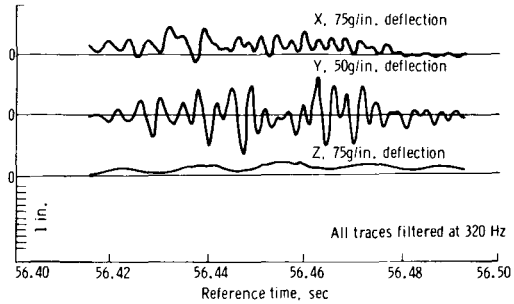
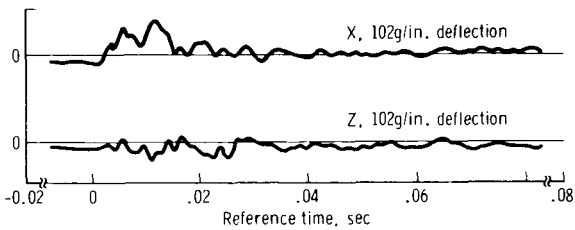


Figure 37. - Boilerplate accelerations at c.g. under conditions of test 63.

Figure 38. - Accelerations at c.g. during test 64 with CM-011.

Traces filtered at 320 Hz from test 61 with BP-1201

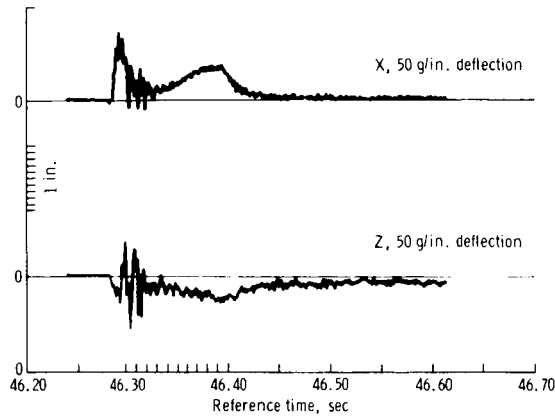


Figure 39. - Boilerplate accelerations under conditions of test 64.

were made with BP-1201 at roll angles between 0° and 180° to establish the stability of askew landings.

The CM-002B was impact tested at a roll angle of 325° and a horizontal velocity of 54 fps. The peak accelerations recorded at the c.g. were 30g in the X axis, 27g in the Y axis, and 11g in the Z axis. The shapes of the acceleration pulses were similar to those of the 0° roll tests and resembled a single pulse of approximately 0.045-second duration that has principal components of X and Z axis accelerations. The accelerations are shown in figure 40. The results of a boilerplate test under similar conditions are shown in figure 41. The CM-002B impact sequence is shown in figure 42.

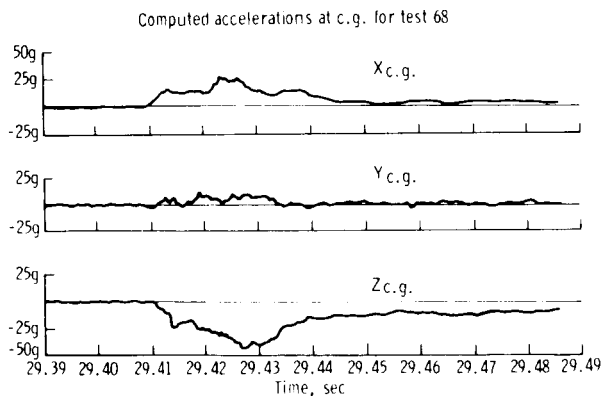


Figure 40. - Accelerations recorded during test 68 with CM-002B.

Askew Landing Tests

As predicted from scale model and boilerplate tests, a roll angle of 180° produced the most unstable landings. Any deviation from the 180° roll condition increased landing stability. From the summation of moments at impact, it can be seen that any shortening of the moment arm between the surface contact point and the c.g. velocity vector is a stabilizing influence. Landings at 180° roll have the maximum positive-pitch moment arm at impact, and 0° roll landings have the maximum negative value. In an askew landing, a rolling moment is produced by the surface contact point being outside the vertical plane that contains the horizontal velocity. Three impact tests

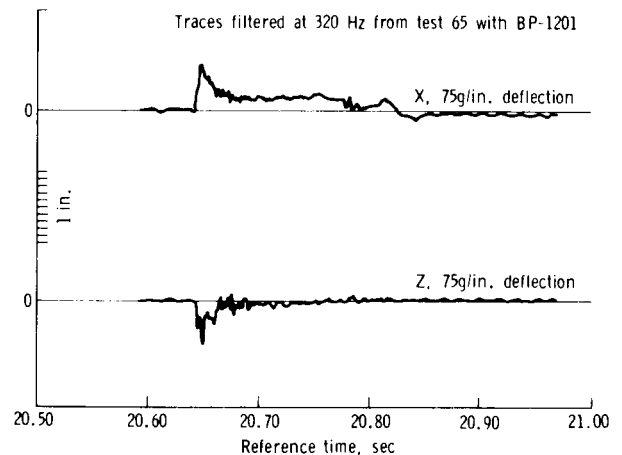


Figure 41. - Boilerplate accelerations under conditions of test 68.

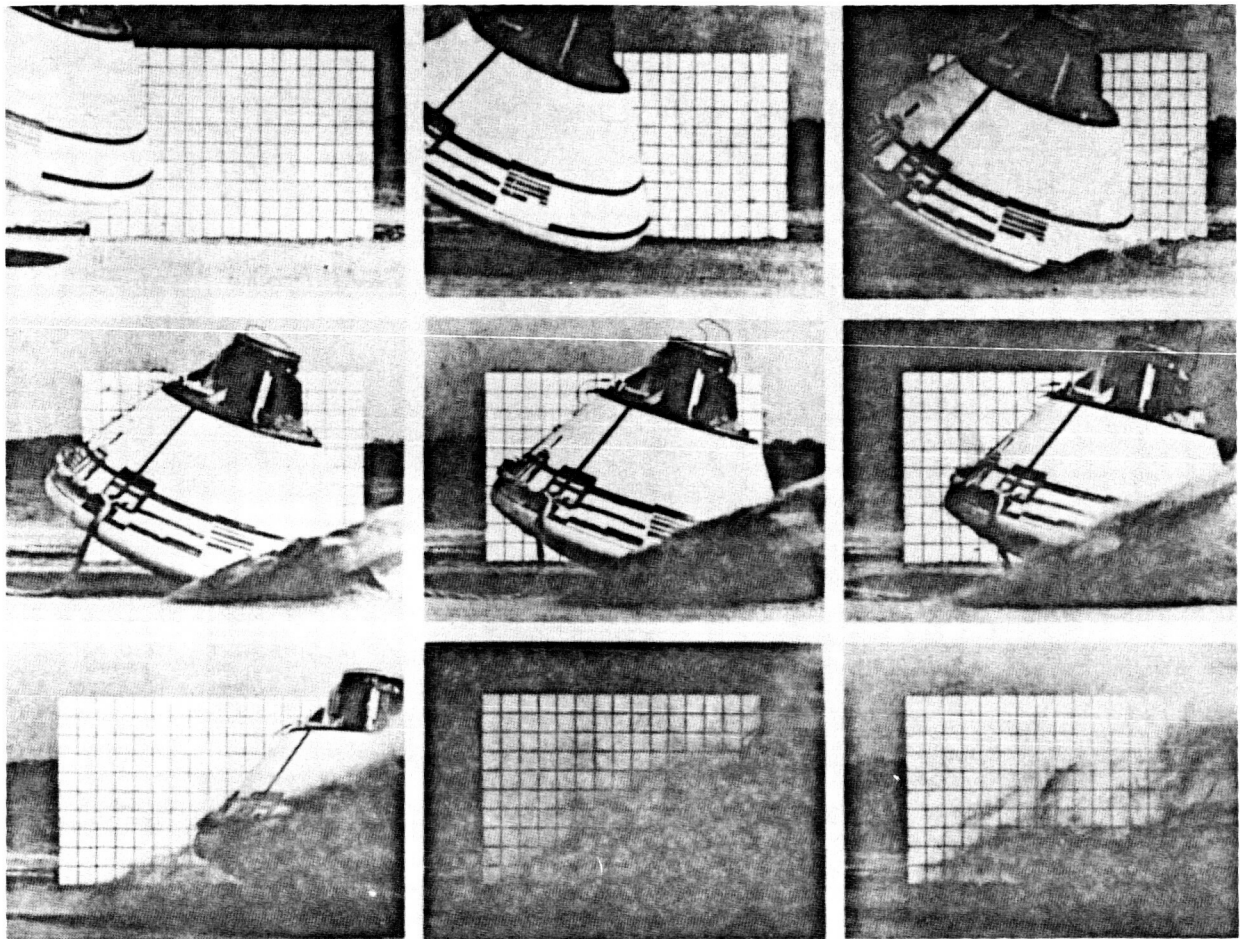


Figure 42. - Landing dynamics of CM-002B during test 68.

Less damage was sustained by CM-002B than by any other spacecraft tested in the program (fig. 43). Damage was limited primarily to the +Z section of the aft heat shield where some slight buckling occurred outside the bolt circle. No damage was apparent on the crew-compartment aft bulkhead. A slight debonding of one sidewall frame occurred.

Damage to Secondary Equipment

The RCS tanks. - One or both RCS oxidizer tanks were crushed or ruptured by the aft-heat-shield ballast during all of the spacecraft-impact tests except test 68 with CM-002B. However, none of the fuel tanks



Figure 43. - Damage to CM-002B in test 68.

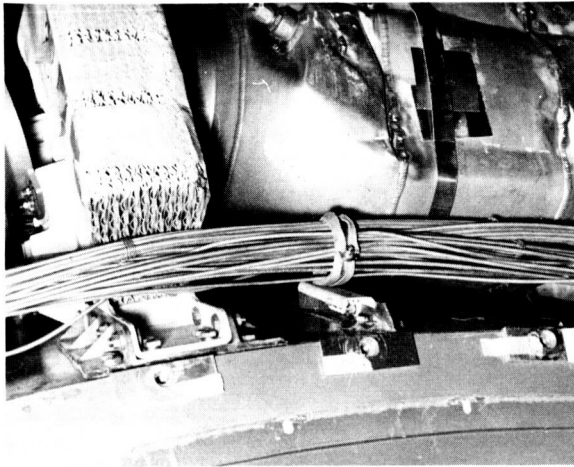
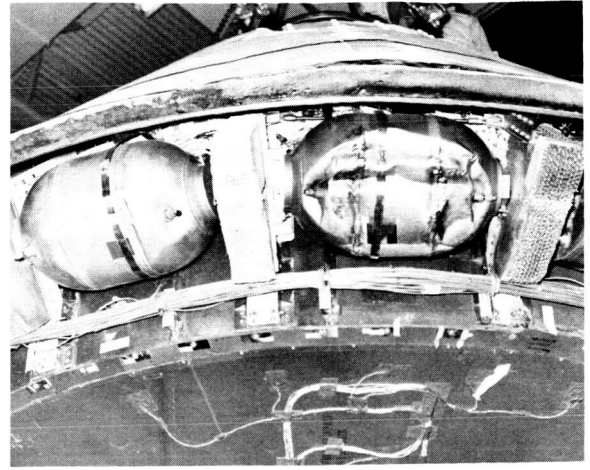
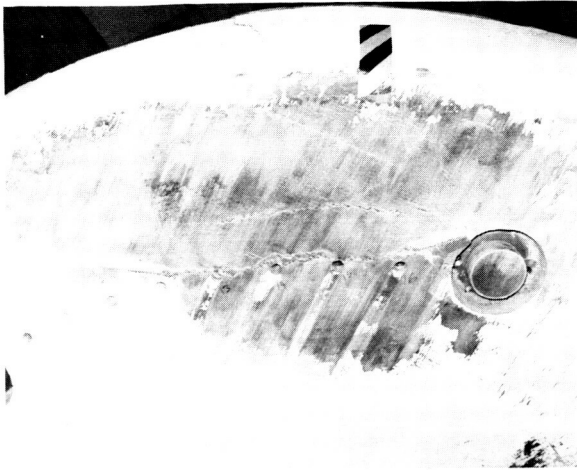


Figure 43. - Concluded.

was crushed to such an extent that spillage of the fluid was imminent. Nothing can be concluded about the possibility of a fire resulting from the rupture of the RCS plumbing. Neither this plumbing nor the type of ballast that is most likely to damage this system (fig. 11) were installed on any of the test vehicles. However, extensive damage in areas containing plumbing is indicative of a high probability of toxic-fume release from the oxidizer tanks and a significant possibility of fire caused by the mixing of oxidizer with the fuel from ruptured lines. In most tests, numerous cracks in the aft bulkhead and sidewall provided routes to the crew compartment for the released fluids and fumes. Typical damage caused to RCS tanks by a land impact is shown in figure 44

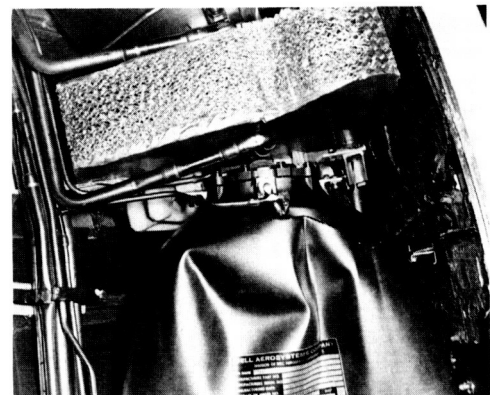
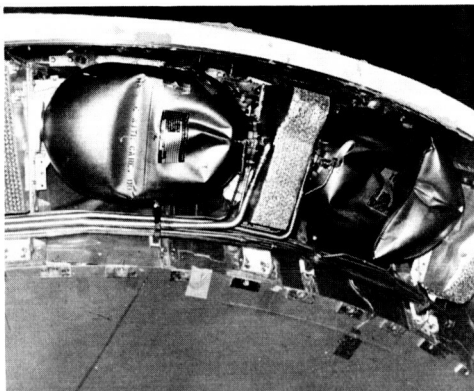


Figure 44. - Typical impact damage to RCS tanks.

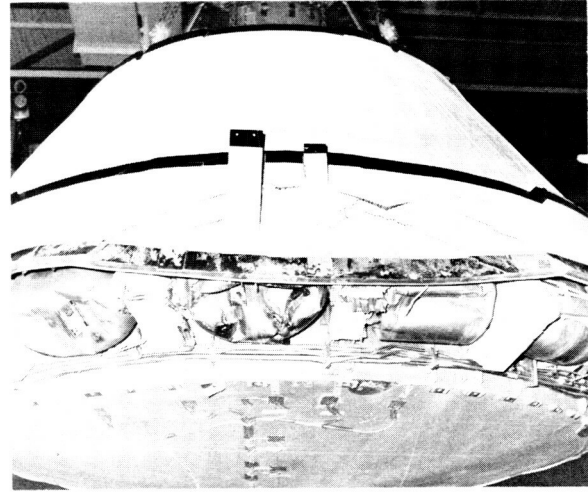
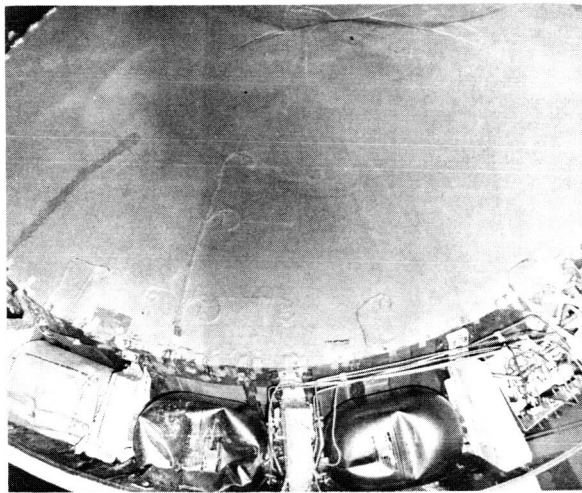
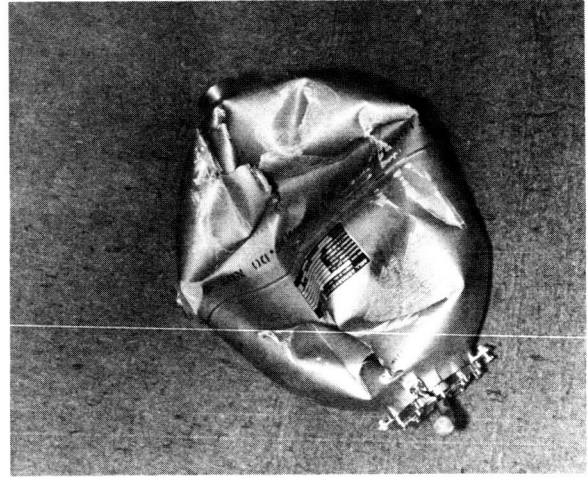
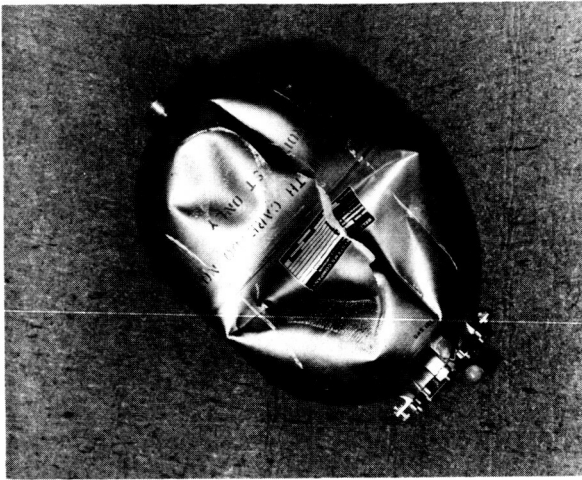


Figure 44. - Concluded.

The oxygen surge tank. - No damage occurred to the oxygen surge tank in any of the tests, and the surge tank retained its pressure of 850 psi during the test for which it was pressurized (test 63 with CM-009). The conclusion was reached that a significant hazard does not exist to the crew from the oxygen tank or its attachment. However, as in the case of the RCS, the plumbing was not installed on any of the test vehicles; therefore, no assessment can be made of possible damage to this hardware.

Crew-Systems-Equipment Performance

In all of the land-impact tests, a time lag existed between the accelerations recorded on the anthropomorphic dummies and crew-couch system and those recorded near the c. g. of the test vehicle. The elasticity of the crew-couch system, which produced the time lag, also recorded higher accelerations than those at the c. g. of the vehicle. The recorded couch-strut loads did not deviate greatly from the design values.

Typical data recorded during a 0° roll landing (with CM-009) and during a 180° roll landing (with CM-011) are shown in figures 45 and 46. The solid-line curves are plots of X axis accelerations experienced at the c.g. of each test vehicle. The dashed lines are crew-couch and dummy accelerations recorded at a location near the vehicle c.g. The fourth curve in figure 46 was generated by a calculation of the rigid-body accelerations put into the couch system by the struts. The calculations were made by adding the X axis components of the strut loads at various times and dividing by the weight of the suspended mass. As the curve indicates, the stroking loads of the struts limited the g force of the couch system to approximately 17g in the X axis. However, the couch and dummy accelerometers recorded 37g and 42g, respectively; however, the acceleration at the c.g. of the vehicle was only 34g. This amplification was experienced by both the unitized and the foldable crew couches.

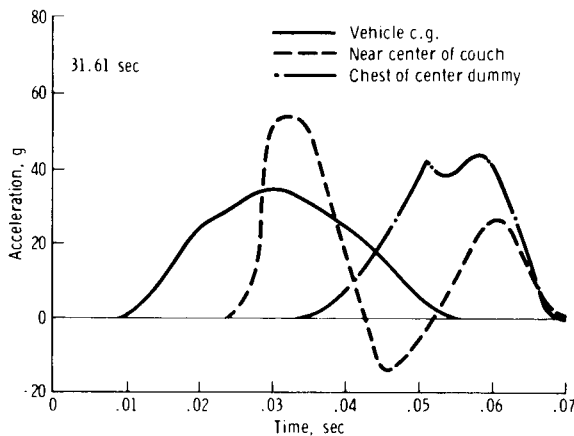


Figure 45. - Accelerations in the X axis during test 31 with CM-009.

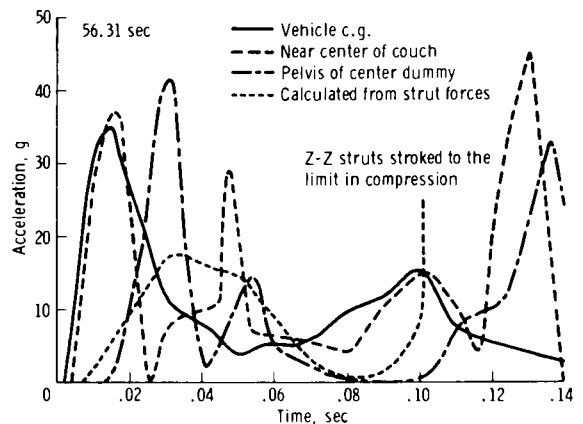


Figure 46. - Accelerations in the X axis during test 64 with CM-011.

The accelerations represented by the couch and c.g. curves are only the X axis component at a particular location. Higher and lower X axis component accelerations were recorded at other points in the couch system. Also, the resultant accelerations were much higher than the associated X axis components.

Another potential crew hazard was revealed during the test of CM-011 when the Z-Z couch struts stroked to their limit in compression as a result of the crushing of the -Z sidewall of the spacecraft. The crew couch was loaded severely and caused the Z axis accelerometer in the chest of the center dummy to record 37.5g. Subsequent modifications of the Z-Z strut design have further reduced their stroking load, which will provide even less protection from stroking to their limit during severe 180° roll landings.

Emergency crew-recovery procedures will be needed if a 180° roll landing occurs. The CM could come to rest in a position that would render the upper-deck-attachment fittings unusable for uprighting. Moreover, the side hatch area may be damaged and prevent the actuation of the hatch-opening mechanism. Access through the docking

tunnel or, in extreme cases, through an opening sawed in the aft heat shield might be required. In any case, expedient removal of the crewmen is mandatory because of the potential presence of toxic fumes and the possible incapacitation of the crewmen as a result of excessive accelerations.

Structural Capability and Stability

Estimates of the structural capability and stability of a CM in a land landing have been derived from this test program (fig. 47). Such estimates are based on the nominal descent rate of 32 fps and the nominal pitch attitude of -27.5° with impact on hard-packed sand.

Horizontal velocities are displayed as concentric circles increasing from zero at the center to 60 fps at the outermost circle. Roll attitude is displayed as the angle between the spacecraft +Z axis (as defined in fig. 13) and the projection of the horizontal-velocity vector into the Y-Z plane. As an example, the test conditions of CM-002B (represented by the black square in the upper-left-hand quadrant) were a horizontal velocity of 54 fps and a roll attitude of 325° . The area shaded by the left-hand diagonal lines represents the structural capability of the CM to withstand various impact conditions. It was derived by assessing the damage caused during the five spacecraft tests and by interpolation between test conditions. The area shaded by right-hand diagonal lines represents the landing stability. It was defined by the relative stability of both spacecraft and boiler-plate tests.

It can be concluded from this figure that the basic structure is adequate for land landings if the horizontal velocity does not exceed 40 fps. If the roll attitude of the vehicle is within $\pm 90^\circ$ of zero roll, the structural capability is equal to or greater than the horizontal wind velocity that constrains the launch of the booster (54 fps).

Probability of Emergency Landing

All data in this report resulted from tests considered representative of emergency land-landing conditions. Such conditions can occur only as a result of a mission abort on the launch pad or during the first 40 seconds of flight. Should such an abort occur, an 83-percent chance exists that the vehicle will impact on land; of these landings, an 88-percent chance exists that the vehicle will not impact on the hard-packed fill material.

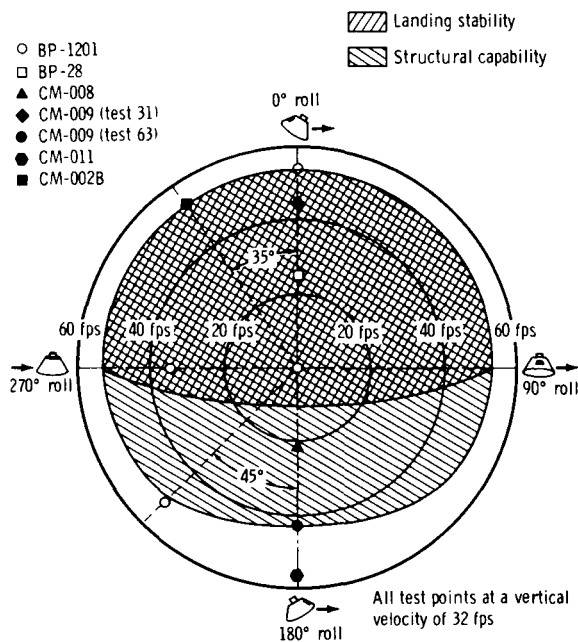


Figure 47. - Land-landing capability as a function of roll angle of a CM.

A 75-percent chance exists that the winds will be less than 43.5 fps, and approximately a 24-percent chance exists that the vehicle will not land near a 180° roll attitude. With these probabilities combined, less than a 5-percent chance exists that an aborted mission will result in a CM landing under conditions as severe as in the tests of CM-009 or CM-011.

CONCLUDING REMARKS

The capability of the Apollo command module to withstand the loads imposed by an emergency land landing is much greater than had been expected. Very little damage can be expected from 0° roll and askew-roll landings that are not close to 180°. Most of these landings should be stable to velocities as high as those that constrain the operation of the launch vehicle.

Most 180° roll landings will be unstable, and extensive structural damage can be expected, even at low horizontal velocities. At horizontal landing velocities in excess of 40 fps, structural failure is a definite hazard to the crewmembers.

In all land landings, a strong probability exists for damage to the reaction control system tanks and plumbing. Damage to this hardware creates the hazards of fire and toxic fumes within the crew compartment.

The oxygen surge tank can be expected to retain its structural integrity during all landings within the ranges of the tested parameters. However, massive damage to the area of the oxygen surge tank plumbing can be anticipated.

Emergency crew-recovery procedures may be needed if a 180° roll landing occurs. The upper deck may be damaged, making it difficult to upright a tumbled vehicle, or the damage to hatch areas may prohibit normal recovery techniques. In any case, expedient removal of the crew is mandatory because of the potential presence of toxic fumes and the possible incapacitation of the crew from excessive accelerations.

Accelerations of 40g to 50g will be experienced in the X and Z axes at the center of gravity of the command module. An approximate 20-percent amplification of these accelerations by the couch system could produce higher values than those prescribed as emergency crew-tolerance levels. Analyses have been performed to optimize the crew-couch struts to minimize the accelerations and provide maximum protection against exceeding the strut stroking capabilities.

Manned Spacecraft Center
National Aeronautics and Space Administration
Houston, Texas, June 6, 1972
914-50-20-17-72

APPENDIX A

INSTRUMENTATION

The identifications and locations of the various transducers installed for the major tests in the land-impact program are shown in figures A-1 to A-24. In general, the figures are arranged by test number and vehicle, but occasionally the same figure is representative of two or more tests and is not repeated under succeeding tests or vehicles.

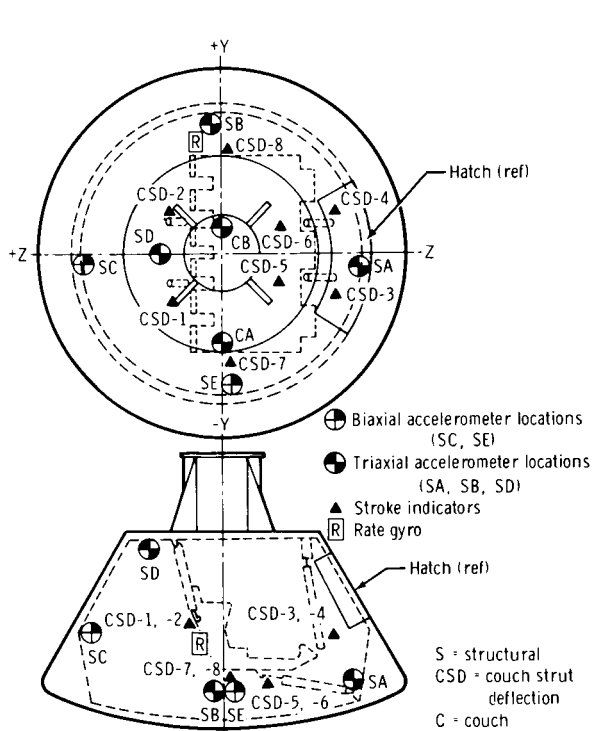


Figure A-1. - Locations of accelerometers and stroke indicators for test 16 with BP-28A.

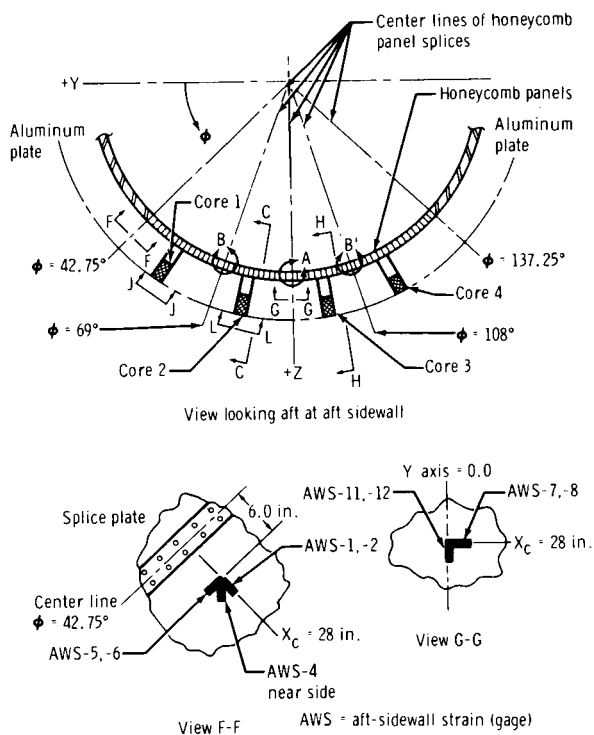


Figure A-2. - Aft-sidewall strain-gage locations for test 16 with BP-28A.

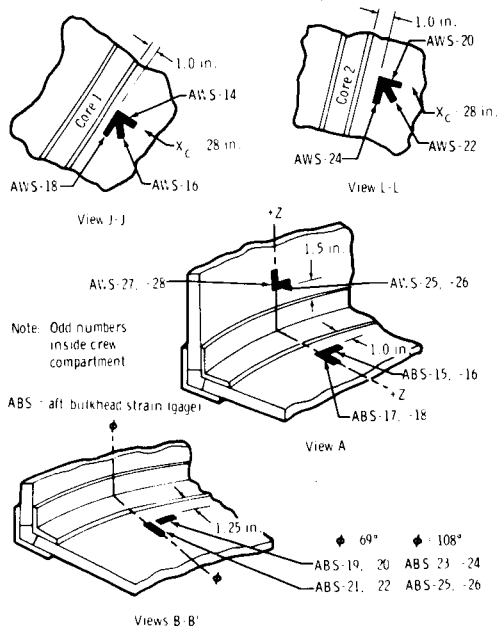


Figure A-3. - Details of aft-sidewall strain-gage locations for test 16 with BP-28A.

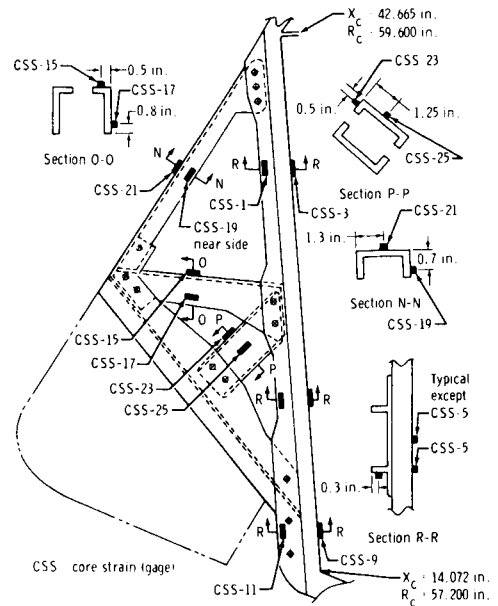


Figure A-4. - Aft-sidewall strain gages at core 2 for test 16 with BP-28A.

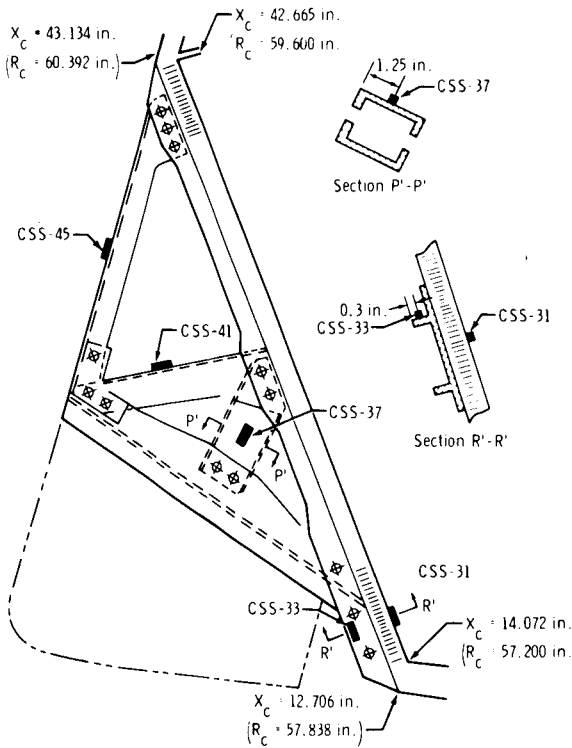


Figure A-5. - Aft-sidewall strain gages at core 3 for test 16 with BP-28A.

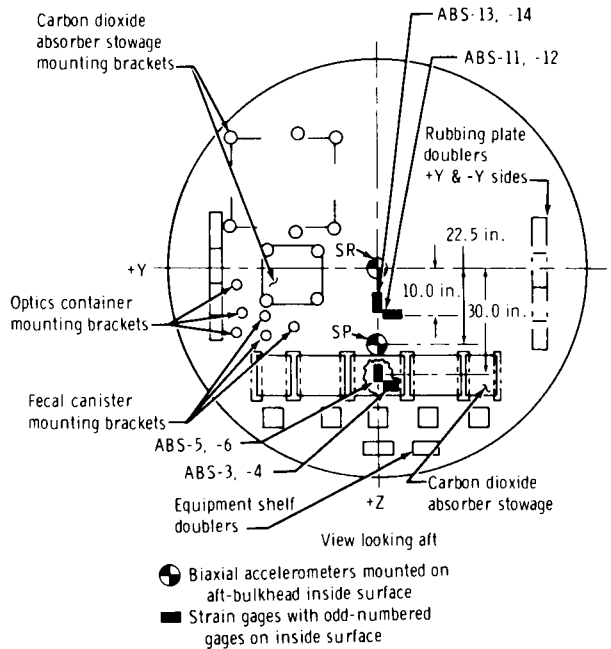


Figure A-6. - Aft-bulkhead equipment and instrumentation for test 16 with BP-28A.

Camera Location and view or type

- A Monorail track - release to impact (10 mm)
- B North accelerator rail - before release (8 mm)
- C Top frame east end - start to release
- D End impact area - parallel to track (10 mm)
- E End impact area - parallel to track (10 mm)
- F Perpendicular to impact (16 mm)
- G Perpendicular to impact (16 mm)
- H Perpendicular to last frame - velocity
- I Perpendicular to roll over (16 mm)
- J Perpendicular to impact (Bell & Howell)
- K Perpendicular to impact (Hulcher)
- L Tracking release to impact (Arriflex)

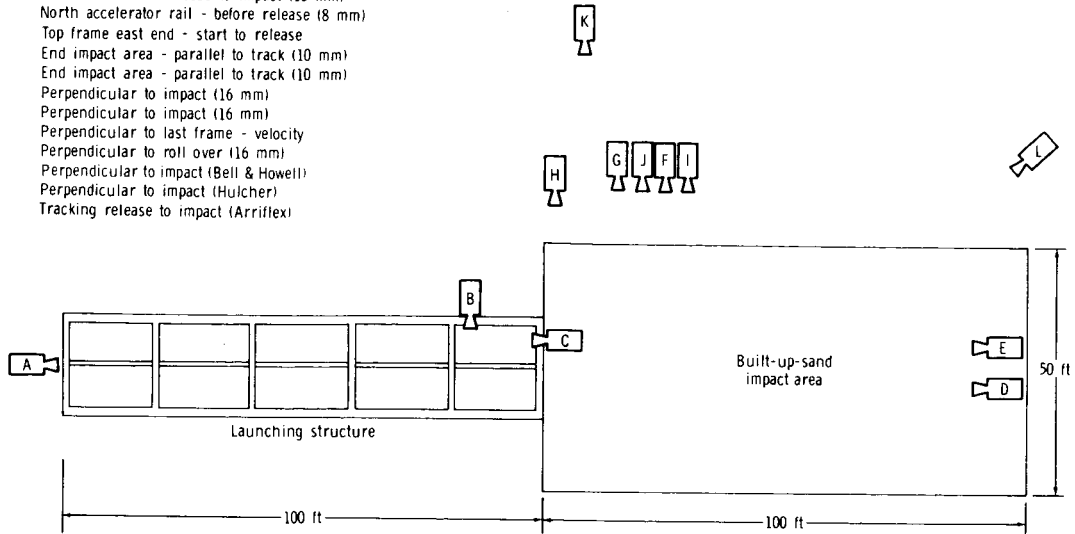


Figure A-7. - Range-camera coverage for test 16 with BP-28A.

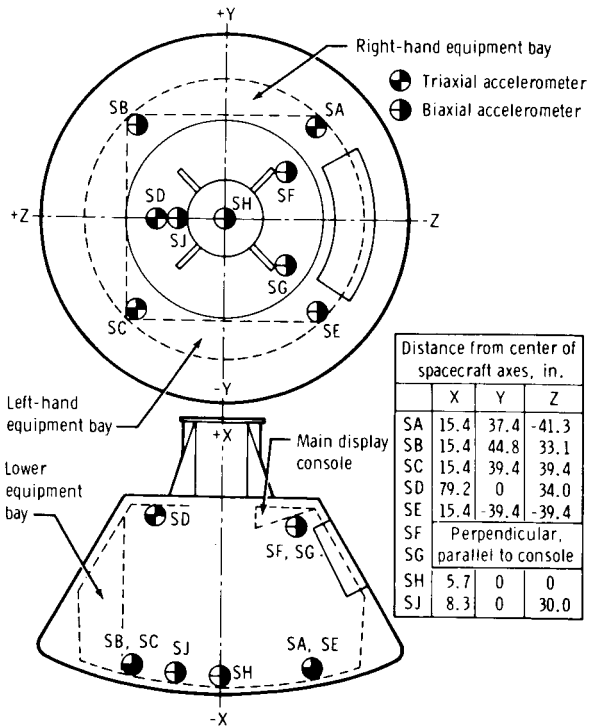


Figure A-8. - Locations of structural accelerometers for test 28 with CM-008.

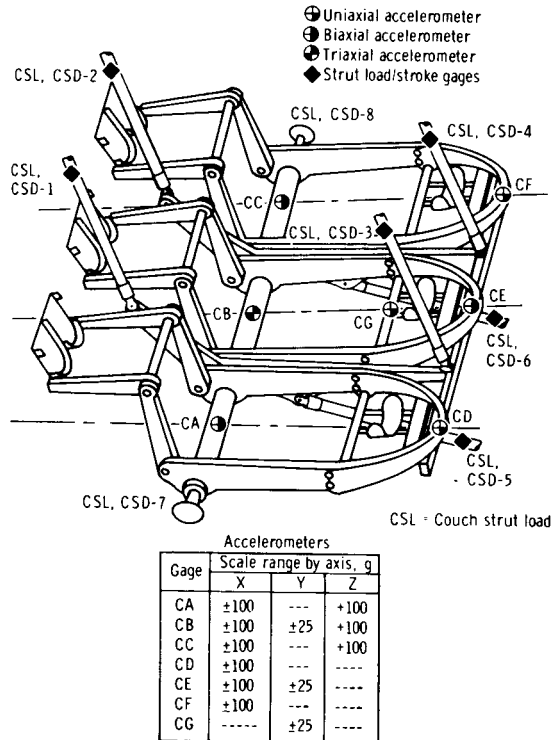
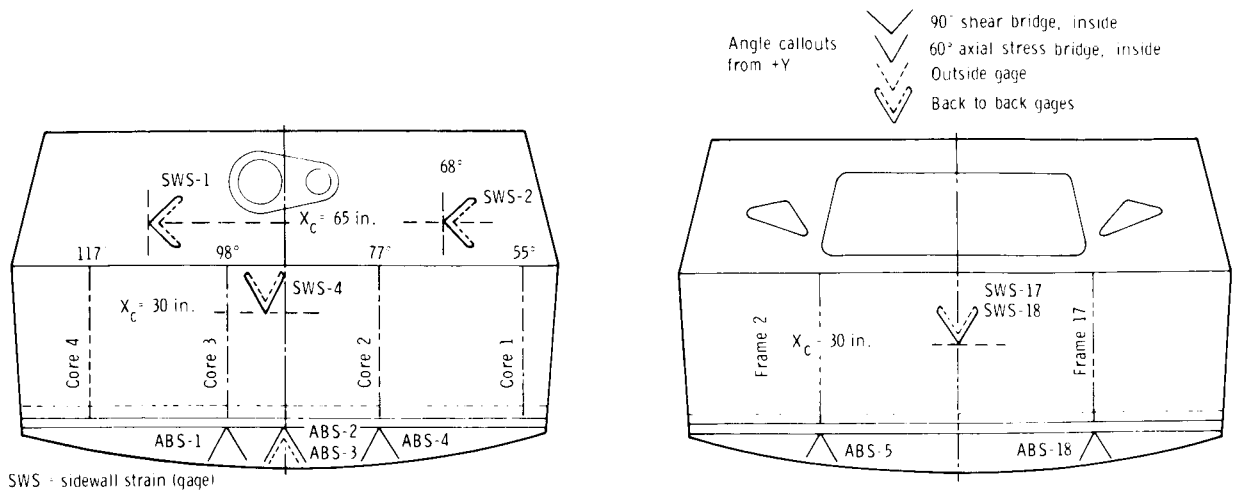


Figure A-9.- Instrumentation of foldable crew couch and support system for test 28 with CM-008 and test 31 with CM-009.



(a) Inside view toward +Z.

(b) Inside view toward -Z.

Figure A-10. - Locations of analog-recorded strain gages for test 28 with CM-008.

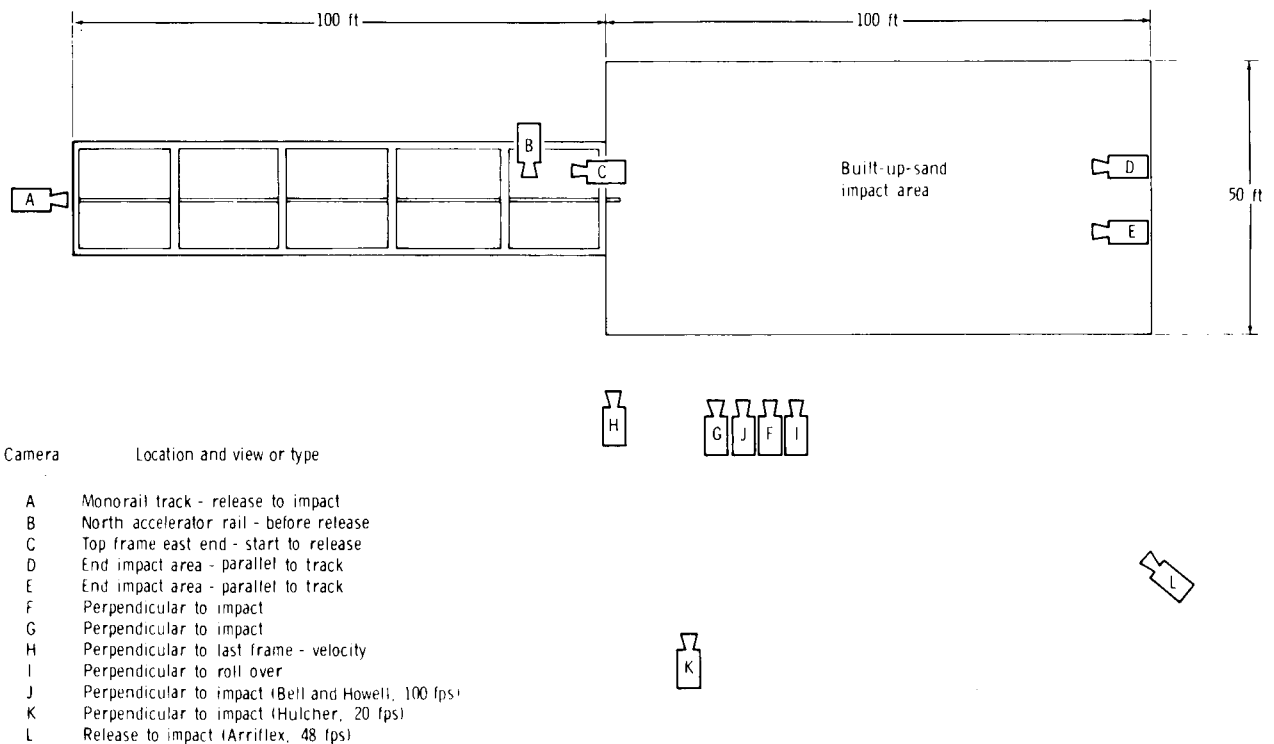


Figure A-11. - Locations and views of range cameras for test 28 with CM-008.

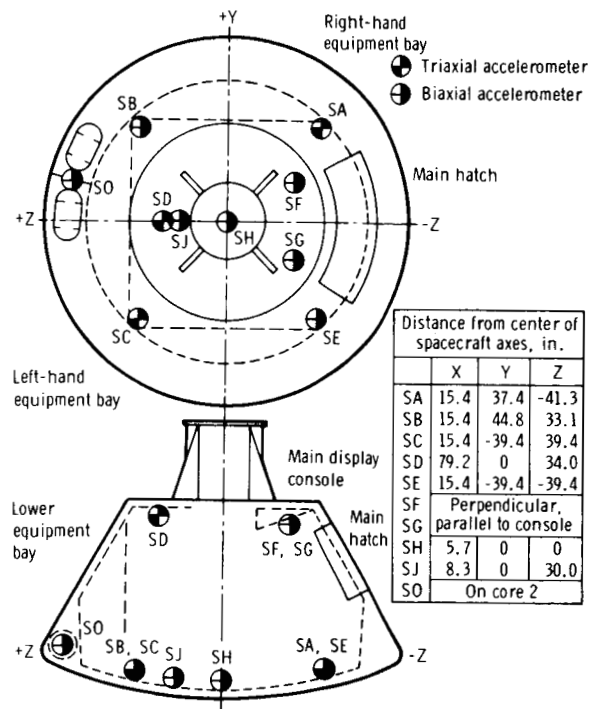


Figure A-12. - Locations of structural accelerometers for test 31 with CM-009.

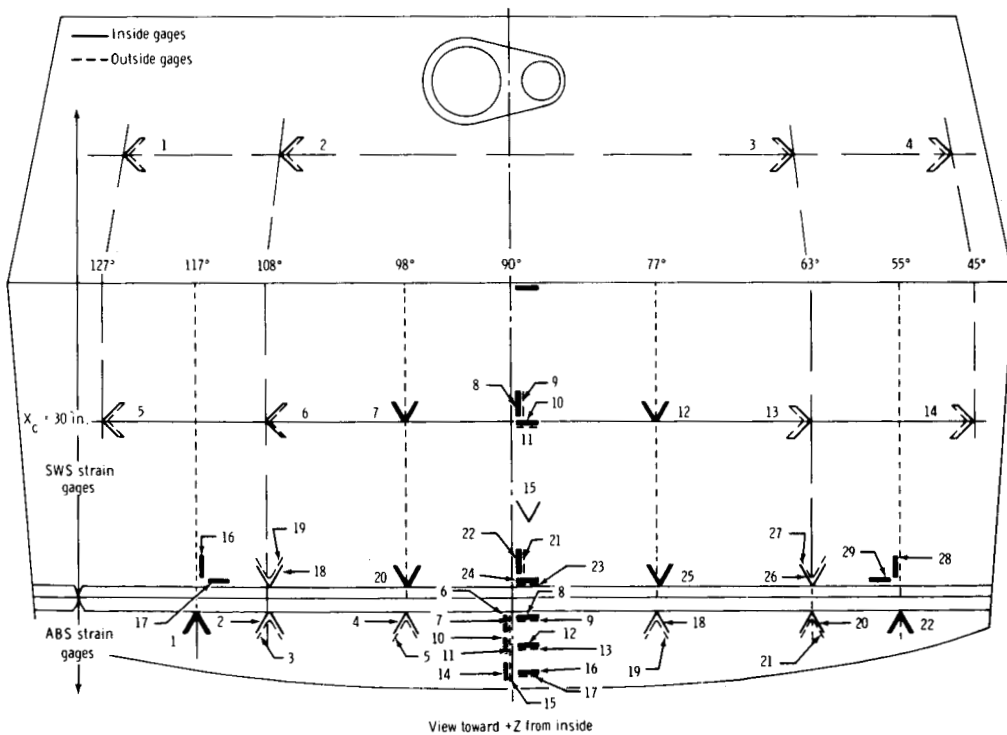


Figure A-13. - Locations of sidewall- and aft-bulkhead strain gages for test 31 with CM-009.

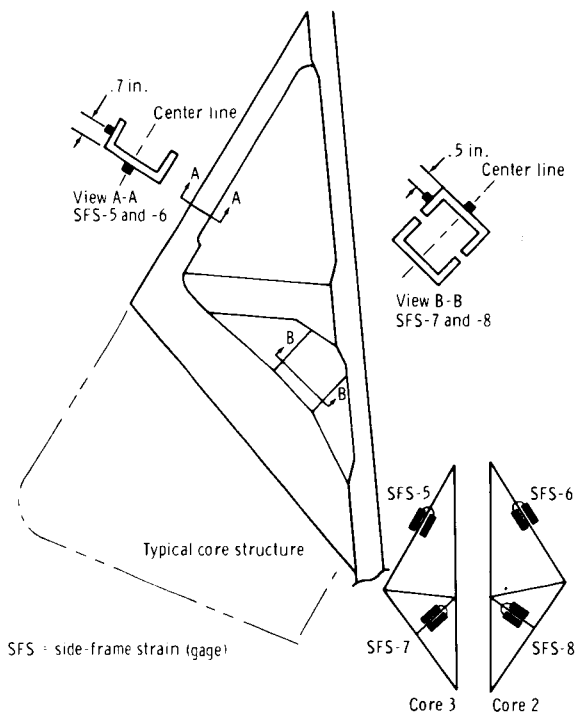


Figure A-14.- Locations of side-frame strain gages for test 31 with CM-009.

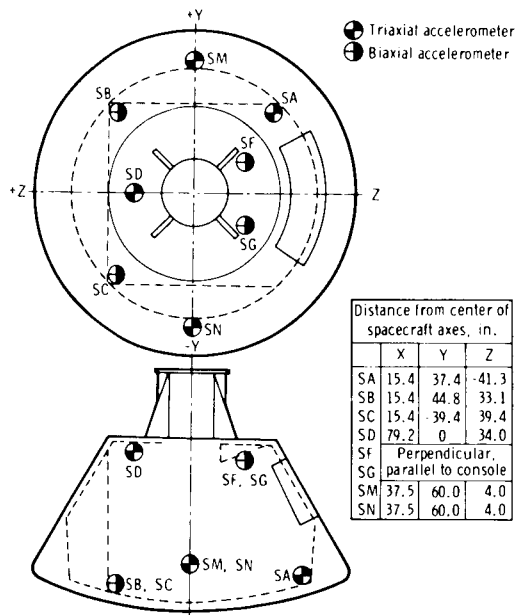


Figure A-16.- Structural accelerometers for test 63 with CM-009 and test 64 with CM-011.

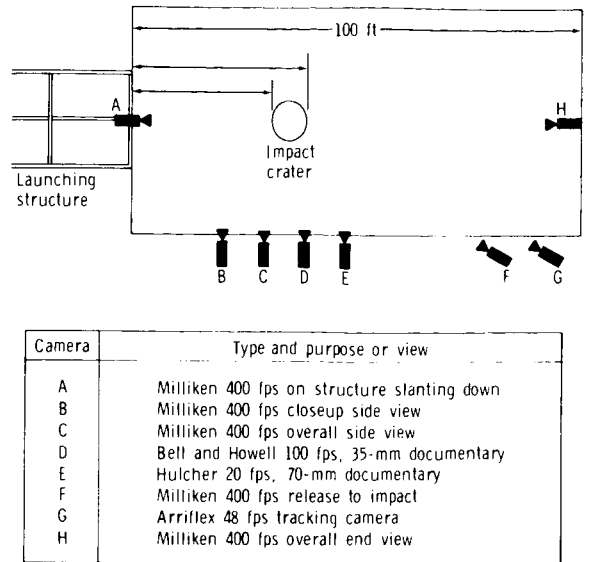


Figure A-15.- Locations of range cameras for test 31 with CM-009.

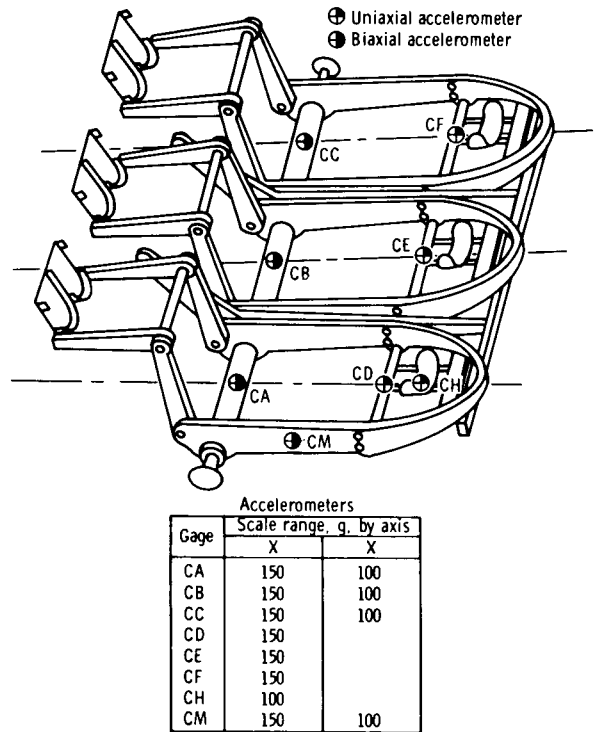


Figure A-17.- Crew-couch accelerometers for test 63 with CM-009 and test 64 with CM-011.

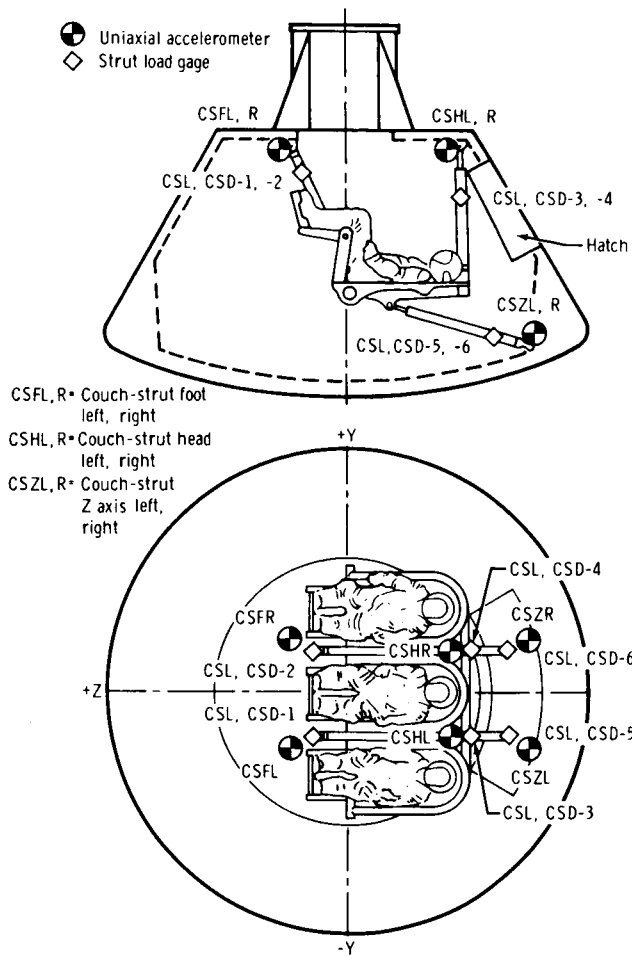


Figure A-18. - Crew-couch strut instrumentation for test 63 with CM-009.

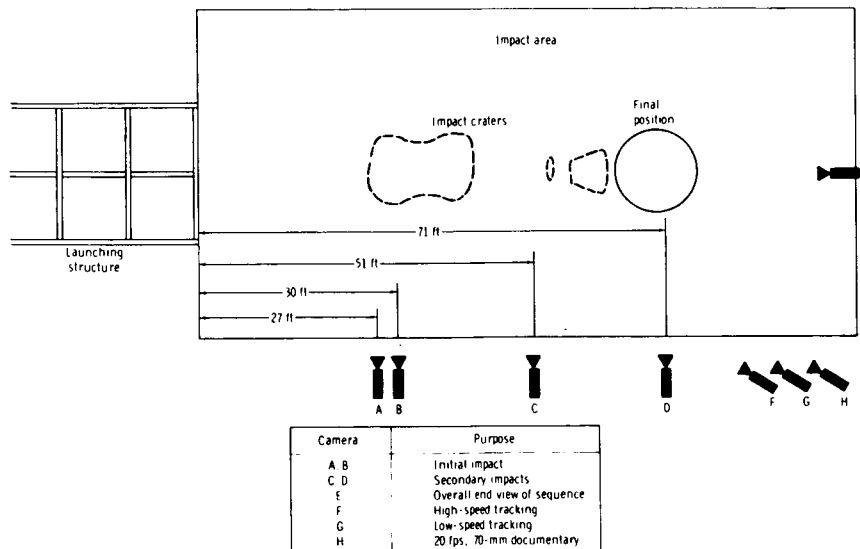


Figure A-19. - Locations of range cameras for test 63 with CM-009.

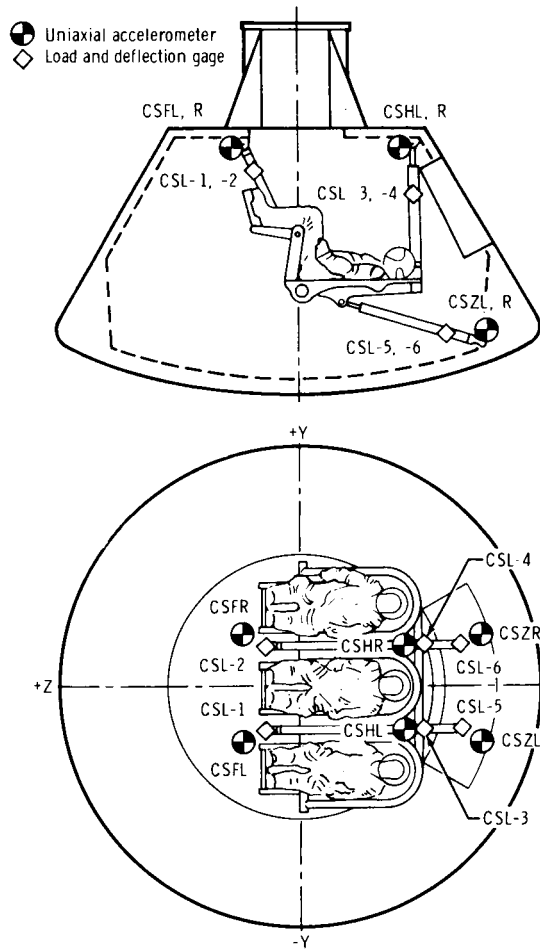


Figure A-20. - Crew-couch strut instrumentation for test 64 with CM-011 and test 68 with CM-002B.

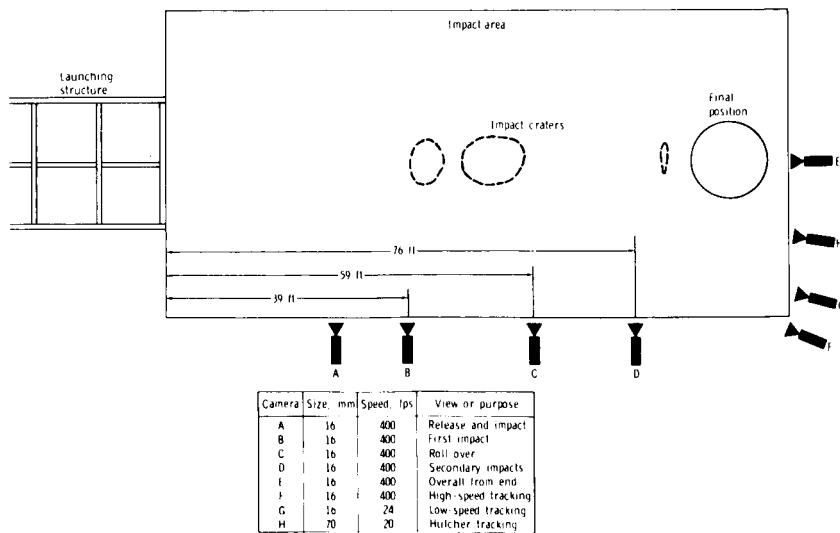


Figure A-21. - Locations of range cameras for test 64 with CM-011.

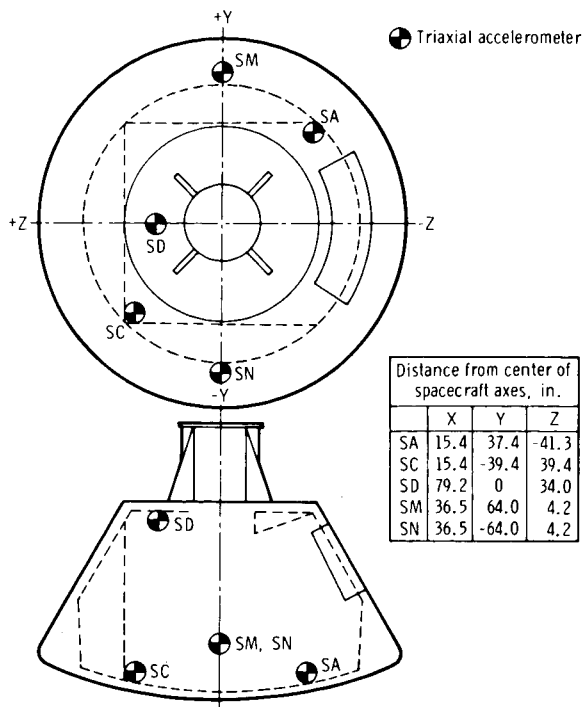


Figure A-22.- Structural accelerometers for test 68 with CM-002B.

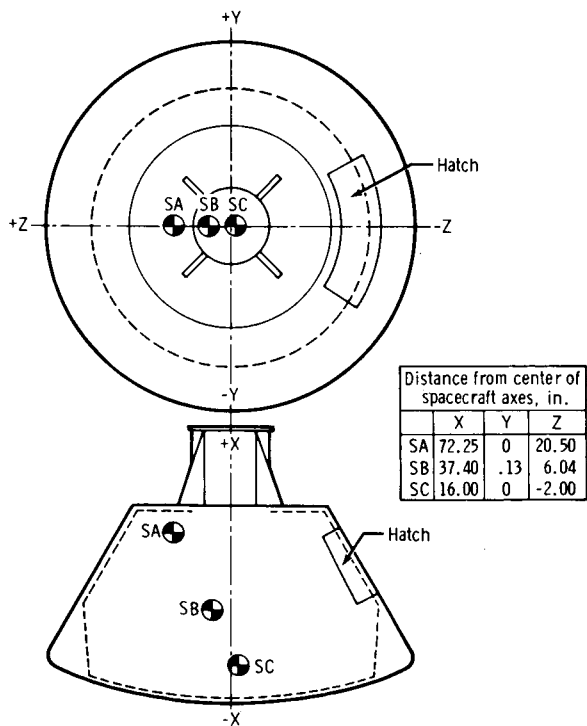


Figure A-24. - Locations of accelerometers in BP-1201.

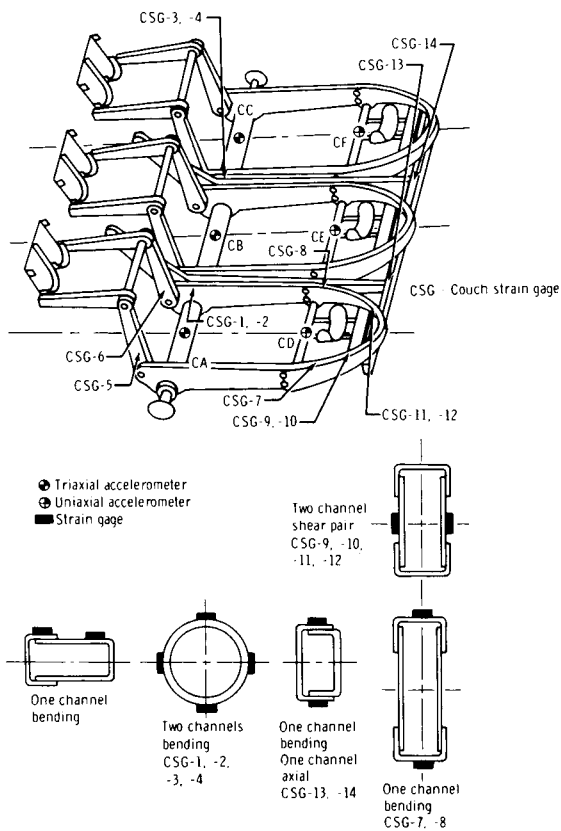


Figure A-23.- Crew-couch instrumentation for test 68 with CM-002B.

APPENDIX B

IMPACT DATA

TABLE B-1. - APOLLO COMMAND MODULE IMPACT TESTS

Test no.	Date	Surface	Attitude, deg			Velocity, fps		File no.	Vehicle
			Pitch	Roll	Yaw	Vertical	Horizontal		
1	5/31/67	Sand pile	27.5	180	0	28	44 to 46	S67-317	BP-002
2	6/23/67	Sand pile	27.5	180	0	28	38	S67-334	BP-002
3	6/30/67	Sand pile	27.5	180	0	28	39.2	S67-337	BP-002
4	7/3/67	Sand pile	27.5	180	0	28	37.3	--	BP-002
5	7/6/67	Sand pile	27.5	180	0	28	51.0	S67-565	BP-002
6	8/8/67	Hard sand	18.5	0	0	38	43.5	S67-417	BP-001
7	8/16/67	Hard sand	18.5	0	0	38	43.7	S67-427	BP-001
8	8/31/67	Hard sand	18.5	0	0	38	43.5	S67-449	BP-1201
9	9/2/67	Hard sand	18.5	0	0	38	43.5	S67-452	BP-001
10	9/7/67	Hard sand	36	0	0	38	43.5	S67-459	BP-1201
11	9/9/67	Hard sand	32.5	0	0	38	43.5	S67-456	BP-1201
12	9/12/67	Hard sand	27.5	0	0	38	43.5	S67-466	BP-1201
13	9/16/67	Hard sand	27.5	0	0	32	25.3	S67-486	BP-1201
14	9/15/67	Hard sand	27.5	0	0	32	17	S67-487	BP-1201
15	9/18/67	Hard sand	27.5	0	0	32	25.6	S67-488	BP-1201
16	9/27/67	Hard sand	27.5	0	0	32	25	S67-491	BP-28
17	10/9/67	Hard sand	27.5	0	0	33	37.8	--	BP-1201
18	10/11/67	Soft sand (15 to 18 in. deep)	27.5	0	0	33	37.8	S67-506	BP-1201
19	10/13/67	Soft sand (24 in. deep)	27.5	0	0	33	40.3	--	BP-1201
20	10/23/67	Hard sand	27.5	180	0	32	25.0	S67-533	BP-1201
21	10/24/67	Hard sand	27.5	180	0	32	43.5	--	BP-1201
22	10/31/67	Hard sand	18.5	180	0	32	25.3	S67-544	BP-1201
23	11/2/67	Hard sand	18.5	180	0	32	43.5	S67-540	BP-1201
24	11/9/67	Hard sand	37.2	180	0	32	25.3	S67-545	BP-1201
25	11/13/67	Hard sand	37.2	180	0	32	43.5	S67-600	BP-1201
26	12/1/67	Hard sand	--	180	0	32	40.5	S67-600	BP-1201
27	12/13/67	Hard sand	27.5	180	0	--	40.5	--	BP-1201
28	1/11/68	Hard sand	31	180	0	32	21.25	S69-009	CM-008
29	2/8/68	Hard sand	27.5	180	0	32	45	S68-83	BP-1201
30	3/1/68	Hard sand	27.5	0	0	32	46	S68-151	BP-1201
31	3/7/68	Hard sand	27.5	0	0	32	42.55	S68-174	CM-009
32 to 60	--	Water	--	--	--	--	--	--	--
61	10/18/68	Land	-27.5	180	0	32.81	54.8	--	BP-1201
62	10/22/68	Land	-27.5	180	0	--	51.3	S68-596	BP-1201
63	10/26/68	Land	-27.5	180	0	--	42.1	S68-603	CM-009
64	10/31/68	Land	-27.5	180	0	--	56.34	S68-613	CM-011
65	11/12/68	Land	-27.5	270	0	--	35.08	S68-629	BP-1201
66	11/13/68	Land	-27.5	225	0	--	51.3	S68-631	BP-1201
67	11/18/68	Land	-27.5	315	0	--	46	S68-623	BP-1201
68	11/26/68	Land	-27.5	325	0	--	54.1	S68-445	CM-002B
69	--	Water	--	--	--	--	--	--	--
70	3/10/69	Sand	-27.5	0	0	32.77	44	No film	BP-1201
71	3/21/69	Sand	-22	0	0	32.65	43.7	No film	BP-1201
72	3/25/69	Sand	36	0	0	32.16	44	70-mm Hulcher	BP-1201
73	3/26/69	Sand	36	0	0	32.39	56.4	--	BP-1201
74	3/28/69	Sand	36	0	0	31.94	29.4	--	BP-1201
75	--	Water	--	--	--	--	--	--	--
76	4/7/69	Sand	27.5	0	0	32.2	44	--	BP-1201
77	4/10/69	Sand	27.5	0	0	31.9	56.2	70-mm Hulcher	BP-1201
78	4/22/69	Sand	27.5	0	0	32.5	31.2	--	BP-1201
79	4/23/69	Sand	18	0	0	32.5	45.2	--	BP-1201
80	5/1/69	Sand	27.5	0	0	32	0	--	BP-1201
81	5/1/69	Sand	27.5	0	0	38	0	--	BP-1201
82	5/26/69	Sand	18	0	0	32	29.5	--	BP-1201
83	5/28/69	Sand	18	0	0	32	58.8	--	BP-1201